Identification and Analysis of the Two *Tau* Paralogues in Zebrafish

Mengqi Chen

Supervised by Michael Lardelli and Frank Grützner

Discipline of Genetics

School of Molecular and Biomedical Science

The University of Adelaide

AUSTRALIA

July 2009

CHAPTER I

Introduction

The microtubule associated protein tau (*MAPT*) is well known for its association with numerous neurodegenerative diseases, including Alzheimer's disease (AD), frontotemporal dementia with parkinsonism linked to chromosome 17 (FTDP-17), progressive supranuclear palsy (PSP), corticobasal degeneration (CBD), Pick's disease, and argyrophilic grain disease (AGD) [1]. Characterized by the formation of pathological filamentous tangles in neurons, the main component of which is hyperphosphorylated tau, these diseases are now collectively termed tauopathies [1]. However, the formation of tau tangles was recognized only as a late histological hallmark of these diseases and was, therefore, of limited interest. The causative relationship between tau dysfunction and these neurodegenerative disorders was not established until 1998, when mutations in the gene encoding tau gene were identified as an autosomal dominant genetic risk for FTDP-17 [2-4]. This breakthrough fueled interest in tau and stimulated a number of investigations on tau function and pathology. Much has now been learned about the tau protein. However, the detailed mechanisms of tau misbehavior under pathological conditions and how it leads to neurodegeneration remain enigmatic. In this review, our current understanding of the role of tau in cell physichology and pathology is discussed. The animal models that have been developed for study of tauopathies are also summarized. Following the review, my research data on the study of two zebrafish endogenous tau genes will be presented and discussed.

1.1 The genetics of *MAPT*

The human tau gene *MAPT* is located on chromosome 17q21 [5], and consists of at least 16 exons [6]. While there is only a single tau gene in humans, it can produce a number of different transcripts through a complex alternative splicing system. Three mRNAs of 2, 6 or 9kb are initially generated from the original pre-mRNA before any proceeding splicing, depending on the maturation stage and type of the neurons [7-10]. The 2kb transcript is ubiquitously expressed. The protein it encodes is not localized to microtubules and thus may not have a microtubule-related function [7] . The 6kb transcript is restricted to neuronal tissue. The 9kb transcript, which includes a particularly large exon 4A (about 752bp in length) , is only expressed in the retina and peripheral nervous system (PNS) [9]. In addition, an internal ribosomal entry site in the human tau 5' mRNA leader sequence has been reported, adding another dimension of complexity to tau regulation [11].

Eight (2, 3, 4A, 6, 8, 10, 13, 14) out of the 16 exons of *MAPT* can be alternatively spliced [12]. Exons 1 to 4 encode a projecting region, which interacts with the plasma membrane. The affinity of the projecting region to the plasma membrane can be modified by the alternative splicing of exons 2 and 3, which produces three different isoforms with zero, one or two 29 amino acid residue inserts in its N-terminal half (referred as 0N, 1N or 2N tau) [13]. Exons 4A to 6 compose a hinge region, which functions as a spacer to determine the distance between the microtubules it associates [14]. Isoforms with exon 4A arise from 9kb transcripts that are restricted to the retina and PNS. Inclusion of the particularly large exon 4A gives rise to ~110 kDa bands on Western blots and almost doubles the distance between adjacent microtubules in cells overexpressing this tau isoform [15, 16]. The C-termini of tau proteins are highly conserved among different species and contain the most important functional domain, known as the microtubule associated domain. This domain, encoded in human *MAPT* by exons 9 to 12,

contains three or four (with or without exon 10) imperfectly repeated tubulin-binding motifs. Depending on the number of the tubulin-binding repeats, the tau isoforms are classified into two major groups, the 3-repeat-tau (3R-tau) group and 4-repeat-tau (4R-tau) group [17, 18]. The inclusion of an additional tubulin-binding repeat in 4R-tau greatly increases its affinity for microtubules. Thus, it is more efficient at stabilizing microtubules compared to 3R-tau [19].

Despite the large repertoire of tau isoforms, only six of them are commonly expressed in adult human brain. These six isoforms are generated by the alternative splicing of exons 2, 3 and 10 [20]. Only the shortest isoform (0N3R) is expressed in the fetus of both humans and rats [8, 21]. However, the isoform profiles of adult human and rodent brains are quite different. In adult human brain, the ratio between 3R and 4R-tau is approximatively 1:1 [8, 22], whereas in adult rodent brain only 4R-tau isoforms are found [21, 22]. The splicing pattern of exon 10 is of particular interest because of its intimate involvement in the pathology of tauopathies. Disruptions of the one to one balance between 3R and 4R-tau are consistently reported in various tauopathies [23-25]. In addition a number of FTD-associated tau mutations can affect the normal splicing of exon 10. These findings implicate that alteration of exon 10 splicing may cause tau malfunction and thus neurodegeneration [1].

1.1.1 Tau mutations in tauopathies

The finding that mutations in *MAPT* can cause autosomal dominantly inherited FTD focused interest on this gene. Since the initial identification of several FTD-associated tau mutations in 1998 [2-4], more than 40 different mutations in either exonic or intronic regions have now been reported (http://www.molgen.ua.ac.be/FTDMutaitons). Despite two mutations in exon

1 (R5H, R5L), all of the remaining mutations occur within or near the highly conserved tubulin-binding domain. These mutations can be classified roughly into two groups: 1) missense and single codon deletions that can alter tau protein sequence and 2) silent and intronic variations that can affect the ratio between 3R and 4R-tau. The missense mutations (eg. G272V, P301L, P301S, R406w, etc.) usually cause a reduction in microtubule-binding ability, impairment of the regulation of microtubule dynamics and elevated propensity for self-aggregation [23, 26, 27]. Splicing mutations (eg. L284, N296, IVS10+3 +11+12+13+14+16, etc.) are found in coding regions and introns. All of them affect the splicing of exon 10 and thus induce an imbalance of isoforms [28]. A few mutations can affect both the amino acid sequence and splicing pattern (eg. N279K). Despite the well established genetic linkage to FTD, patients carrying *MAPT* mutations can also display PSP, CBD and (in a rare case) AD-like symptoms [29, 30].

Genomically, the *MAPT* locus is in a ~1.8Mb block of linkage disequilibrium, which can be divided into two major haplotypes known as H1 and H2 [31]. The more common H1 haplotype shows a strong association with sporadic PSP [31, 32], CBD [32, 33] and one of the H1 sub-haplotypes has been recently associated with AD [34]. It appears that the H1 and H2 haplotypes have different effects on transcript expression. The H1 haplotype shows a higher level of expression of *MAPT* overall than H2 [35, 36]. Recently, it was also reported that the H1 haplotype increases the inclusion of exon 10 by about 43% and decreases the inclusion of exon 3 by two-fold compared to H2 [37, 38].

The association of *MAPT* polymorphisms with various tauopathies indicates that dysfunction of tau protein alone may be sufficient to induce neurodegenerative tauopathies. Furthermore, the investigation of how these mutations confer susceptibility to tauopathies highlights the importance of

the precise transcriptional regulation of *MAPT*, especially, the regulation of exon 10 splicing. Unfortunately, however, the precise mechanism of how these polymorphisms affect transcriptional regulation and how alteration of transcription may lead to neurodegeneration remain to be determined.

1.1.2 The regulation of *MAPT* splicing

As mentioned above, multiple tau isoforms are generated from the single *MAPT* gene by alternative splicing [12]. Rigorous regulation of tau splicing appears to be critical for its normal neuronal functions, given that an imbalance of isoform expression is often accompanied by dysfunction of tau protein in various tauopathies. In addition, disrupted regulation of splicing is a universal characteristic of various tauopathy-associated mutations [28]. Therefore, the regulation of tau alterative splicing is of great interest.

In adult human brain, six major isoforms are generated from the alternative splicing of exons 2, 3 and 10 [39]. Isoform expression is developmentally regulated *via* employment of a set of cis-elements and trans-acting factors. The default splicing pattern of exon 2 is inclusion and skipping of exon 2 can be stimulated by most splicing regulators, such as SRp30c, htra2beta1, PTB and SRp55 [40]. In contrast, the default splicing behavior of exon 3 is exclusion. Thus, the inclusion of exon 3 requires the help of an activator and is enhanced by the pre-inclusion of exon 2 during splicing. In fact, exon 3 has never been found without exon 2 [41, 42].

The splicing regulation of exon 10 is quite complex and has attracted most attention due to its strong relevance to several tauopathies [28]. The splicing of exon 10 can be influenced by the sequences of its flanking introns [43]. The 5’ splicing site of exon 10 is a hot spot for multiple *MAPT* mutations,

most of which increase the inclusion of exon 10 in transcripts [2, 44]. It has been proposed that this is due to increased access of U1 snRNP or another factor to this splicing site [2, 4]. The mutations destabilize a putative loop structure in this region [44, 45] or increase the sequence complementarity between the transcript and the splicing factor [46]. In addition to the 5' splicing site, splicing of exon 10 can also be affected by its exonic sequences. At the 5' region of exon 10, three enhancers have been identified, including a SC35-like enhancer, a polypurine enhancer (affected by mutations N279K and K280del), and an AC-rich element (affected by silent mutation L284) [47, 48]. Following these enhancers, two weak silencers have been identified. These silencers can be disrupted by mutations N296H, N296N and N296del [49].

A number of splicing regulators are involved in tau splicing. For example, splicing regulator TrAβ can increase skipping of exon 10 by interacting with the polypurine enhancer [50], while most SR and hnRNP proteins can inhibit splicing of exon 10 [43]. Noticeably, the activity of these regulators can be moderated by phosphorylation and several kinases have been suggested to be involved. For example, overexpression of cdc2-like kinase can promote exon 10 skipping [51], while repression of GSK-3β activity increases exon 10 inclusion [52].

1.2 Posttranslational modification of tau

Tau protein undergoes several forms of posttranslational modification, including phosphorylation, truncation, ubiquitination, glycosylation, glycation and nitration. Aside from glycation which has only been found in tauopathy-affected brain, these modifications occur both under normal and pathological conditions. However, the level of posttranslational modification seems to be significantly elevated in most tauopathies [53].

1.2.1 Phosphorylation

Among all the above posttranslational modifications, phosphorylation has been the most widely studied because the tau filaments found in tauopathies are usually hyperphosphorylated and this abnormal hyperphosphorylation status is linked to tau toxcity [54]. Normally, each mole of brain tau contains 2-3 moles of phosphate while the phosphorylation level of tau is 3- to 4-fold higher in AD-affected brain compared to age-matched controls [55, 56]. Therefore, much endeavour has been devoted to untangling the role of tau hyperphosphorylation in AD and other tauopathies.

Functionally, phosphorylation reduces the affinity of tau for microtubules. Therefore, it affects microtubule assembly negatively. This mechanism enables tau to regulate microtubule dynamics and axonal transport *via* its phosphorylation state [57]. The phosphorylation level of tau in normal adult brain is relatively low, while abnormal hyperphosphorylation is consistently observed in various tauopathies [58]. Interestingly, however, hyperphosphorylation of tau protein is not necessarily pathological. In the fetus, tau proteins are hyperphosphorylated at sites overlapping some of those identified under pathological conditions [58]. Recently, it has also been reported that hyperphosphorylation of tau is observed in small mammals during hibernation (, although the sites that are phosphorylated during hibernation represent only a subset of those in AD-affected brains) [59, 60]. These hyperphosphorylated forms of tau form paired helical filaments (PHF) like those found in tauopathies, and synapse loss is also observed. However, unlike in tauopathies, all of these changes are reversible after hibernation [59]. Collectively, these observations imply that hyperphosphorylation of tau alone may not be sufficient to induce neuronal toxicity and that temporary hyperphosphorylation of tau may serve certain physiological functions. In

fact, recent evidence has suggested that tau hyperphosphorylation may induce the cell cycle in neurons [61, 62] and thus may play a critical role in neuron plasticity and maturation during embryogenesis [63].

1.2.2 Truncation

Tau proteins truncated at both/either the N- and/or C-termini are found in NFTs in tauopathy-affected brain [64, 65]. Evidence from antibody binding tests implies that truncation may play a role in the conformational transformation of tau proteins from unfolded monomers to misfolded tangles [66, 67]. N-terminally truncated tau can be detected specifically by an antibody called tau-66 and is found at a late stage of tangle formation [66]. C-terminus cleavage usually occurs after residues D421 and E391 [68, 69]. The removal of the C-terminal tail of tau proteins largely improves tau aggregation *in vitro* [70]. Both the N- and C-terminal cleavage events appear to be performed by caspases and occur soon after the formation of tau tangles [67, 71, 72]. This might contribute to stabilizing further this folded conformation of tau proteins [67].

1.2.3 Ubiquitination

It has been found that PHF-tau isolated from brains affected by tauopathy is polyubiquitinated, primarily at site L48 [73, 74]. Modification of ubiquitins at L48 serves as a signal for the degradation of these tagged tau proteins *via* an ATP-dependent ubiquitin-proteasome pathway [74, 75]. *In vitro* study has shown that this mechanism involves the participation of the C-terminus of the HSP70-interacting protein (CHIP-Hsp70) which can interact with Hsp70 to target the misfolded tau [76, 77]. Overexpression of CHIP can improve the degradation of the hyperphosphorylated tau induced by increased GSK-3β activity or decreased PP2A activity in both N2A cells and rat brains.

However, it does not seem to improve memory in rats [78]. In addition, CHIP also degrades both phosphorylated and nonphosphorylated tau in normal rat brain [78]. In AD-affected brain, the level of CHIP seems to be elevated compared to control [79]. However, the activity of the proteasome is somehow inhibited, resulting in the deposition of ubiquitinated tau and the formation of PHFs and tangles [80]. Therefore, the impairment of the ubiquitin-proteasome system might explain why overexpression of CHIP alone failed to rescue the memory deficit in the study above.

1.2.4 Other modifications

In addition to the posttranslational modifications described above, an enhanced level of N-glycosylation [81] and nitration [82] has also been reported in AD affected brains. In addition glycation of tau proteins was found in AD-affected but not normal brains [83]. In contrast, the level of O-GlcNacylation appears to decrease in AD brains since it shares the same sites as phosphorylation [84]. Therefore, it is assumed that O-GlcNacylation of tau may normally control the level of tau phosphorylation by a competition mechanism [85].

1.3 The dysfunction of tau protein

The dysfunction of tau observed in multiple tauopathies is characterized mainly by two kinds of imbalance. On one hand, the precise regulation of alternative splicing of tau mRNA appears to be disturbed resulting in a shift in isoform balance between 3R and 4R-tau [28]. On the other hand, the phosphorylation level of tau proteins is significantly elevated, due to a disrupted balance in the activities of tau kinases and phosphatases. In addition, alteration in other forms of posttranslational modification such as truncation, glycosylation, glycation and nitration can be observed. These changes prompt the normally soluble tau proteins to aggregate into insoluble paired helical filaments (PHFs) and tangles *via* a series of conformational

changes [53]. The distribution of tau proteins in neurons is also altered. Tau proteins are principally found in distal axons [86, 87]. However, in most tauopathies, hyperphosphorylated tau proteins are preferentially deposited in the somatodendritic compartments [88]. In addition, the impaired interaction between tau and microtubules triggers a set of downstream events such as failure of axonal transport, compromised signal transduction, loss of the cytoskeleton, etc. [1].

1.3.1 Altered splicing

As mentioned above, the composition of tau isoforms is often altered in tauopathies. In cases of PSP and CBD [24, 25, 89], only 4R-tau is detected in tau depositions, while in Pick's disease, the tau tangles are composed mainly of 3R-tau [90]. The alteration of tau isoform production is more complex in FTD, where the balance between 3R and 4R tau can shift towards either side, depending on the relevant mutations. In most cases, FTD-associated mutations increase the ratio of 4R-tau by about 2 to 10 fold [91]. However, in cases of mutations K257T, L266V, G272V on K280del, predominantly 3R-tau is found in tau deposits [92]. In some cases, such as those with mutations V337M and R406W, both 3R and 4R-tau are found in NFTs [93, 94]. In AD, the issue of isoform content is more controversial. Early results showed that the ratio between 3R and 4R-tau in tangles in AD remains close to 1:1 as in normal human brain [95]. However, a recent study revealed that the involvement of 3R and 4R tau differs in each neuron. According to Togo et al., NFTs in the early stages of AD can be made of either 3R or 4R or both tau isoforms in a neuron-specific manner [96]. Nevertheless, the above observations implicate that a shift of the balance of 3R and 4R isoforms to either side can induce neurodegeneration. Under this mechanism, it would seem that the toxicity of tau protein may be caused by disruption of isoform content rather than overexpression or repression of one specific kind of

isoform.

Interestingly, in contrast to the precisely maintained 1:1 ratio between 3R and 4R-tau in adult human brain, predominantly 4R-tau is expressed in adult rodent brain [97]. Tau knock-out/knock-in (tau-KOKI) mice expressing exclusively wildtype human 2N/4R isoforms do not develop any significant phenotype [98]. However, expression of all six human tau isoforms in a tau negative mouse model led to abnormal tau hyperphosphorylation and aggregation similar to that observed in AD [99]. These findings suggest that tau regulation has changed significantly during evolution and casts doubts on whether we are truly able to faithfully reproduce tauopathies by expressing human tau in transgenic rats, especially when attempting to untangle the puzzle of how the alteration of isoform content contributes to tauopathies.

1.3.2 Hyperphosphorylation

As mentioned above, abnormal tau hyperphosphorylation is recognized as a major character of tauopathies. To date, more than 40 phosphorylation sites have been identified [100]. Phosphorylation at different sites of tau proteins appears to convey different functional alterations. For example, phosphorylation at residues S262, Y231 and S235 decreases the affinity of tau for microtubules by ~ 35%, ~25% and ~ 10% respectively [101]. Phosphorylation at residues S199/S202/Y205, Y212, Y231/S235, S262/S356, and S422 may cause abnormal association of tau with other microtubule-associated proteins (MAPs) and interfere with their functional interaction with microtubules [102]. Phosphorylation at S396 or S422 promotes the tendency of tau proteins to self-aggregate [64]. Collectively, it seems that phosphorylation in the proline rich domain of tau proteins mainly impairs their ability to promote microtubule assembly, whereas, phosphorylation at the C-terminal tail enhances self-aggregation [103].

The hyperphosphorylation of tau proteins in tauopathies is the combined result of an overactivation of kinase and inhibition of phosphatase. In vitro, more than ten kinases have been shown to phosphorylate tau proteins [104]. These kinases can be classified into two groups, regarded as proline-directed protein kinases (e.g. ERK1/2, cdc-2, CDK-2, cdk-5, etc.), and nonproline-directed protein kinases (e.g. CaMKII, PKA, PKC, etc), based on the types of residues that are phosphorylated [104].

Among the multiple kinases that have been shown to be involved in tau phosphorylation, the role of GSK-3β in the development of AD (the most common tauopathy) is of central interests. In vitro studies have shown that GSK-3β can effectively phosphorylate tau proteins at multiple sites that are seen to be phosphorylated in the hyperphosphorylated tau filaments of AD-affected brains [105, 106]. Both the expression level and activity of GSK-3β are elevated in AD-affected brain. An in vivo study showed that over-expression of GSK-3β can induce tau hyperphosphorylation and neurodegeneration in mice [107]. In addition, polymorphism in the promoter of GSK3 has been reported to be a risk factor for late-onset AD [108].

The activity of GSK-3β can be regulated by its phosphorylation state. Phosphorylation on S9 of GSK-3β inhibits its activity [109]. It is observed that a decline of PI3K/AKT signaling, which causes overactivation of GSK-3β, has been observed to induce tau hyperphosphorylation and PHF formation [110]. In addition, inhibition of PI3K by PKC results in sustained activation of GSK-3β, and thus, tau hyperphosphorylation [111]. GSK-3β can also be inactivated by an ERK signal less efficiently when compared to a PI3K/AKT signal [110, 112].

Additionally, the phosphorylation of tau by GSK-3β can be stimulated

significantly when tau is pre-phosphorylated by other kinases. In rat brain, pre-phosphorylation of residue S214 of tau by PKA enhances the subsequent phosphorylation at residues S202, S396 and S404 by GSK-3β, as demonstrated by sequential application of PKA and GSK-3β inhibitors [113]. Phosphorylation of tau by other kinases at sites such as S198/199/202 and Y231 has also been shown to prime tau for further phosphorylation such as by GSK-3β [100].

Cdk5 is another major tau kinase. It has been implicated in the development of tauopathies by the observation that p25, the activator of Cdk5, accumulates in sporadic AD-affected brains [114]. However whether Cdk-5 actually plays an important role in tauopathies remains controversial. A study of transgenic mice overexpressing human p25 under the control of the neuron-specific enolase promoter showed that overactivation of cdk5 led to tau hyperphosphorylation [115]. However, in another study where transgenic p25 was transcribed from a cytomegalovirus promoter (pCMV), no significant elevation of tau phosphorylation or neuron death was observed [116]. Similarly, Cdk5 and its activator p35 failed to show any significant effect on tau pathology in a *Drosophila* model [117]. In another transgenic mouse model where the p25 is transcribed from the Ca2+/calmodulin-dependent kinase II promoter, tau hyperphosphorylation was also absent in young transgenic mice. However, in old animals, tau hyperphosphorylation was observed together with an elevated activity of GSK-3β [118]. The diverse results from different studies may be due to the fact that the network of Cdk5 interactions is quite complex and alteration of cdk5 activity can cause a set of downstream events that might somehow affect tau phosphorylation indirectly. Nonetheless, despite the extensively studies that have been performed, the role of cdk5 in tauopathies remains obscure.

In vitro studies have shown that a number of phosphatases, including PP-2A, PP2B, PP-1 and PP-5 can dephosphorylate tau at multiple sites [119]. Among them, PP-2A might be the most important in terms of involvement in tauopathies. Approximately 71% of total tau dephosphorylation is conducted by PP-2A and a decreased level of PP-2A expression and activity has been reported in AD-affected brain [120, 121]. Inhibition of PP2A causes tau phosphorylation at sites correlated with AD both *in vitro* and *in vivo*. Moreover, it has also been shown that the binding of PP2A to tau can be reduced by several FTDP-17 associated mutations [122].

1.4 Multiple hypotheses of the role of tau in tauopathies

1.4.1 Gain of toxic function vs loss of function

Dysfunction of tau proteins has been observed in a number of neurodegerative diseases. A crucial role for pathological alteration of tau proteins in these diseases has been well established by evidence from biopsies, genetic studies, biochemical analysis and various animal models. However, two important questions remain to be answered: 1) How does the observed tau dysfunction lead to neurodegeneration, especially in a spatially selective way in different tauopathies? 2) What is the direct trigger of such pathological alteration of tau proteins?

To address the first question it is important to discuss whether dysfunctional tau proteins exert their toxicity through a loss-of-function or a gain-of-function mechanism? Since abnormal hyperphosphorylation and misfolding of tau proteins largely deprives them of the ability to stabilize microtubules, (which correlates well with observations of impaired cell morphology, axonal transport and trafficking in the affected neurons, [123-126]), it is tempting to assume a loss-of-function mechanism in tau-mediated neurodegeneration. This assumption is further supported by the

observation that MT-stabilizing drugs can enhance neuron survival in transgenic mouse tauopathy models [127, 128]. However, this assumption is challenged by the absence of neurodegeneration in tau knockout mice [129]. More surprisingly, depletion of tau expression seems to render neurons resistant to Aβ-induced neurodegeneration [130]. In the tau knockout model, it appears that tau function might be compensated for (at least partially) by other microtubule-associated proteins [129]. Thus, loss of tau function alone seems to be insufficient to cause neurodegeneration.

On the other hand, the finding that cognitive impairment in tauopathies is correlated with increasing levels of tau deposition implies a gain-of-function mechanism for toxicity. Tau aggregation has been shown to be toxic to neuronal cells and this toxicity can be reversed by drugs that inhibit tau aggregation [131, 132]. However, several *in vivo* studies showed only a weak causative role for NFTs in neuronal toxicity. In an elegant study, transgenic mice expressing repressible human P301L mutant tau displayed neuronal loss and behavioral impairment with accumulation of NFTs in hippocampus in an age-related manner. Suppression of the expression of mutated tau ameliorated the memory deficits and prevented progressive neuron loss. However, the NFTs continued to accumulate [133]. Similarly, treatment of tau P301L transgenic mice (JNPL3) with an ERK2 inhibitor reduced the phosphorylation level of tau and prevented motor impairments, while neurofibrillary tangle counts were not decreased [134].

These observations now lead us to a hypothesis that the toxicity of tau may be due to soluble hyperphosphorylated tau rather than the NFT depositions. This hypothesis appears to fit well with the evidence from studies described above and is further supported by the observation that the reduced microtubule density seen in AD-affected brain appears to be unrelated to the

location of PHFs [135]. In *Drosophila* models expressing wild-type or mutant human tau, hyperphosphorylation of tau proteins is observed together with a reduced lifespan, axon impairment and neuron loss, while tau filaments are absent [136]. It has been shown that abnormally hyperphosphorylated tau not only loses the ability to stabilize microtubules but also sequesters other microtubule associated proteins such as MAP1 and MAP2 [137]. Given that an increased level of MAP1a is observed in tau knockout mice [125], it is likely that hyperphosphorylation of tau exerts its toxicity by a combination of loss of its own function and gain of a toxicity function that compromises the function of other MAPs that might otherwise be able to compensate for loss of tau function. Under this scenario, the formation of tau tangles may be a mechanism that reduces the toxicity of soluble hyperphosphorylated tau.

1.4.2 Synergistic interactions with Aβ

In AD (the most prevalent tauopathy) the accumulation of intracellular tau tangles is observed together with the deposition of amyloid beta peptide (Aβ). The spatial overlap of these two histological pathologies implies a functional linkage [138]. The well-known amyloid cascade hypothesis suggests that tau dysfunction is a downstream consequence of the deposition of Aβ. This hypothesis has now been challenged by observations that tau pathology is also seen in a number of other tauopathies without the presence of Aβ deposition and that carrying a tau mutation alone can induce neurodegeneration [2]. Therefore, it seems that tau dysfunction can also be triggered by factors other than Aβ. However, amyloid beta oligmers remain an important inducer of tau dysfunction as indicated by a number of independent studies.

An *in vitro* study showed that exposure of neurons to filamentous Aβ induced tau phosphorylation [139, 140]. Injection of Aβ peptide directly into the brain

of transgenic mice possessing tau mutations aggravates the tauopathies [141]. Additionally, in comparison to transgenic mice overexpressing only mutant tau, mice expressing both the Amyloid Precursor protein, APP, (from which Aβ is derived) and *tau* mutations develop more tangles in their brain. NFT pathology is notably increased in their limbic system and olfactory cortex, and extended to the subiculum, hippocampus and occasionally isocortex, regions that rarely appear affected by tauopathy in the tau single mutation model [142]. Consistently, passive Aβ immunotherapy has been shown to clear selectively the early tau pathology in a triple transgenic AD mouse model [143, 144]. Other research has shown that an N-terminal antibody against Aβ can reduce the activation of GSK-3β and thus lower the level of tau phosphorylation both *in vivo* and *in vitro* [144]. On the other hand, suppression of tau expression can protect wildtype or transgenic mice carrying APP mutations from Aβ-induced toxicity without reducing the Aβ level [130, 145]. Altogether, it appears that amyloid beta is a trigger that induces downstream dysfunction of tau protein, which then causes neurodegeneration.

1.4.3 Cell cycle re-entry, another potential upstream event of tau dysfunction and neurodegeneration?

Recently, cell cycle re-entry has been proposed as an early event of neurodegeneration in tauopathies. Mature neurons, which account for the majority of the neuron population in adult brains, are normally quiescent. However, a noticeable upregulation of various mitotic markers is observed in the neurons of patients and several animal models with tauopathies [146-148]. Despite this upregulation, no actual mitosis has been detected, indicating a failure to complete the cell-cycle [149]. Thus it is proposed that this re-entry into the cell cycle leads to neuronal death [150].

The alteration of cell cycle control in tauopathies might be triggered by

increased oxidative stress, which is consistently observed in these tauopathies [151]. In addition, several *in vitro* studies have shown that Aβ oligmers are able to induce cell cycle re-entry [152, 153]. In a transgenic mouse model (R1.40), cell cycle re-entry events occur 6-8 months before formation of detectable Aβ deposition. The occurrence of cell cycle re-entry events in this model can be delayed by a reduction of Aβ concentration and completely blocked by elimination of beta secretase activity [154].

Tau proteins are substrates of cyclin dependent kinases, CDKs. A correlation between significantly increased levels of phosphorylation at CDK-directed phosphorylation sites in tau that are affected in tauopathies has been observed during mitosis [155]. Therefore, it is possible that the aberrant hyperphosphorylation of tau proteins is an effect of pathologically re-activated cell cycling. This idea has been supported by the observation of AD-like tau hyperphosphorylation and conformational change in neuronal cells, when these cells are forced to re-enter the cell cycle by expression of the c-MYC and ras oncogenes [156]. More excitingly, in a transgenic mouse model where cell cycle re-entry was triggered by the expression of the simian virus 40 large T antigen (TAg) oncogene, a neurodegenerative phenotype developed with the accumulation of plaque-like Aβ deposits and hyperphosphorylated NFTs [157].

Interestingly, a recent study showed that expression of human mutant tau protein in a Drosophila model caused activation of the cell cycle [158]. Similarly, a study in mice showed that overexpression of normal tau protein can induce neuronal cell cycling [61]. Therefore, if tau dysfunction can be an inducer and an effect of cell cycle re-entry (as implied by the evidence above), a neuron entering this feedback loop at either point would be driven to neurodegeneration.

1.5 Animal models of tauopathies

1.5.1 *Drosophila*

Drosophila is a convenient and powerful model for studies in animal genetics. The nervous system of Drosophila is relatively much simpler than that of humans. Thus it might not faithfully model complex tau pathology as observed in humans. However, the simplicity of its nervous system also brings many advantages. For example, every neuron in the *Drosophila* nervous system can be mapped, which largely facilitates the analysis of neuron migration, synaptogenesis and cellular function [159, 160]. In fact, *Drosophila* models have provided some interesting insights into the mechanism of tauopathies.

There is no identifiable tau ortholog expressed in *Drosophila* but a microtubule-associated protein called DMAP-85 exists, which can stabilize microtubules and which shares some sequence homology with human tau [161]. Introduction of wildtype human tau into *Drosophila* can alone induce age-dependent neurodegeneration. However, the degeneration does not correlate with the formation of intracellular tau tangles [136]. This observation indicates that formation of NFTs may not be an obligatory step for tau toxicity.

Another interesting study investigated the role of three potential tau kinases (GSK-3β, CDk5, MAPK) in tau pathology. It showed a decrease of toxicity of mutant tau that is resistant to MAPK-directed phoshpohorylation compared to wild-type tau in Drosophila. In contrast, mutant tau that is resistant to GSK-3β activity retained toxicity. The Cdk5 did not affect tau toxicity in this model [117]. These experiments provided important information about how kinases activities affect tau toxicity.

1.5.2 Mouse

Despite the crucial role of tau proteins in neurons, the two existing tau knockout mouse lines do not display identical neurodegenerative phenotypes. Significantly delayed neuron maturation was observed in hippocampal cultures as judged by axonal extension. The lag in neuron maturation can be rescued by expressing human tau [125]. The lack of a physical phenotype in tau knockout mice might be due to the compensatory effect of MAP1a, which is upregulated in both tau knockout models [125, 129]. In fact, a *MAPT* and *MAP1a* double knockout mouse model displayed a lethal phenotype and showed suppressed neurite elongation of cultured hippocampal neurons [162].

In transgenic mice, overexpression of a certain kind of wildtype human tau isoform *via* a cDNA vector resulted in hyperphosphorylation of tau proteins. However, NFTs were seldom detected unless the mice were at a very old age [163]. Recently, transgenic mouse models using genomic DNA constructs instead of cDNAs have been established. The obvious advantages of such models are that 1) they eliminate any bias caused by use of exogenous promoters; 2) they allow the expression of all six tau isoforms generated from alternative splicing in an otherwise normal mouse physiological environment [99, 164]. In a genomic tau model where all six human tau isoforms are expressed on a mouse *Mapt* -/- background, hyperphosphorylation of tau proteins and formation of NFTs is observed. As mentioned above, the tau isoform profile in adult mice brain is different from that in humans. Thus, the phenotype induced by expression of wildtype human genomic tau is probably a consequence of altered tau isoform composition [99].

Transgenic mice with FTDP-17 associated mutations display different

degrees of neurodegeneration, motor impairment and memory decline depending on the mutations and the promoters employed. Abnormal hyperphosphorylation is universally found. NFT formation in neurons and, occasionally, in glial cells was also reported in most cases. However, tauopathies like progressive neuron loss were only observed in some lines [163].

A triple transgenic line (3xTg) carrying MAPT P301L, PS1M146V and APPswe mutations has been established to mimic an AD phenotype. This transgenic line displays accumulation of both tangles and amyloid beta in a manner closely resembling human AD [165]. In addition, double transgenic models expressing wildtype or mutated tau with tau-related kinases have also been constructed. These models have provided insights into the mechanism of abnormal tau hyperphosphorylation [58].

1.5.3 Zebrafish

The zebrafish has become a popular animal for studies in genetics. Transgenic zebrafish expressing the FTDP-17 mutant form of human tau were generated in 2002 [166]. GFP was attached to the C-terminal of the tau protein. The htGFP fusion protein retained the ability to assemble and stabilize microtubules in standard turbidity assays and was shown to be a better phosphate substrate than endogenous tau. To achieve neuron-specific expression of htGFP, the zebrafish neural-specific GATA-2 promoter was employed. Expression of the htGFP gene began about 18-20 hours after injection and the zebrafish began to exhibit AD-like cytoskeletal pathology by 48 hours after injection. The study also observed that expression of GSK-3β can be detected early after fertilization in zebrafish brain, indicating that the transgenic zebrafish may serve as a valid model in which to investigate tau phosphorylation [166].

Another research group used an eno2 promoter to produce transgenic zebrafish models of tauopathy. Human 4R-tau isoforms were placed downstream of this promoter. Stable transgenic zebrafish lines were established and showed widespread CNS expression of tau at a level comparable to that in human brain. Accumulations of human 4R-tau were found in neuronal cell bodies of the transgenic zebrafish [167].

The tractability of the zebrafish embryo makes it a promising vertebrate model for large-scale drug selection. In a recent study, a transgenic zebrafish line that expresses human P301L mutated tau in neurons was established. A Gal4/UAS-based bidirectional expression system was employed, which allows the co-expression of tau P301L and the fluorescent DsRed reporter from the same promoter. Therefore, the tau P301L positive cells can be conveniently identified by DsRed flourescence in living embryos. This transgenic line displayed pathological hyperphosphorylation and self-aggregation of tau. Increased neuronal loss can be observed within 24hpf. The model has been used to test the activity of different GSK-3β inhibitors *in vivo* [168].

1.6 Aim of the Research Project

The zebrafish embryo has been demonstrated to be a powerful animal model for genetic analysis due to the combination of many valuable characteristics such as optical clarity, rapid growth, fertility and easy genetic manipulation. In addition, it shows great potential in drug screening [169]. Zebrafish embryos have already been employed in the study of Alzheimer's disease and other tauopathies. However, despite the establishment of several transgenic zebrafish lines expressing human wild type or mutant tau [166-168], no investigation of endogenous tau in zebrafish has yet been reported. Therefore,

in an attempt to further the usage of zebrafish as an animal model for the study of tauopathies, an analysis of the endogenous tau of zebrafish was performed. We sought to provide biological information on endgenous zebrafish tau, including its pattern of expression during development and it physiological function, as well as to develop antibodies to allow the detection of endogenous zebrafish tau protein.

1.7 Summary of papers I and II and links between them

The first manuscript details the identification of two genes, *mapta* and *maptb* in zebrafish that are paralogues of human *MAPT*. These two genes were formed by an ancient duplication of an ancestral tau orthologue. In this manuscript, the complex RNA splicing patterns of the two *mapt* genes are described. The expression patterns of the two genes during embryogenesis are also reported. Interestingly, study of their RNA splicing patterns showed that one gene expresses isoforms containing mainly 3 tubulin binding repeats (3R isoforms) while the other gene expresses isoforms containing mainly 4-6 tubulin binding repeats (4-6R isoforms). In humans, the 3R and 4R tau isoforms are generated from the single tau gene *via* alternative splicing. Failure to maintain a one to one ratio between these two isoform classes is associated with various neurodegenerative disorders. Therefore, the separation of 3R between 4-6R isoforms in two zebrafish *mapt* genes may facilitate the investigation of how the number of tubulin binding repeats affects tau function.

The second manuscript describes the analysis of two polyclonal antibodies raised to detect specifically each of the two tau proteins in zebrafish. In addition, it also presents an initial functional study of both tau proteins. We show that injection of mopholinos inhibiting translation of *mapta* that encodes 4-6R tau isoforms, at a high concentration causes a phenotype of

distortion of rostrocaudal axs including notochord and disorganization of somites. In contrast, the *maptb* gene, (which encodes mainly 3R tau), appears to be essential for axonal outgrowth from trigeminal ganglion neurons.

CHAPTER II

Research Paper I

Complex splicing and neural expression of duplicated tau genes in zebrafish embryos.

Authors:

Mengqi Chen[1,*], Ralph N. Martins[2,3,4] and Michael Lardelli[1]

Affiliations:

1. Zebrafish Genetics Laboratory, Discipline of Genetics, School of Molecular and Biomedical Sciences, The University of Adelaide, Adelaide SA 5005, Australia.

2. Centre of Excellence for Alzheimer's Disease Research and Care, School of Exercise, Biomedical and Health Sciences, Edith Cowan University, Joondalup, WA 6027, Australia.

3. Sir James McCusker Alzheimer's Disease Research Unit, Hollywood Private Hospital, Nedlands, WA 6009, Australia.

4. School of Psychiatry and Clinical Neurosciences, University of Western Australia, Crawley, WA 6009, Australia.

*** Corresponding author:**

Mengqi Chen, Zebrafish Genetics Laboratory, School of Molecular and Biomedical Sciences, The University of Adelaide, Adelaide SA 5005, Australia. Tel. (+61 8) 83034863, Fax. (+61 8) 83034362, email: mengqi.chen@adelaide.edu.au

Journal of Alzheimer's Disease, manuscript accepted for publication on 22nd March, 2009

STATEMENT OF AUTHORSHIP

Complex splicing and neural expression of duplicated tau genes in zebrafish embryos.

Journal of Alzheimer's Disease (Manuscript accepted 22 March 2009)

Mengqi Chen (Candidate)

Performed all experimentation apart from where Michael Lardelli contributed (see below). Wrote the manuscript and acted as corresponding author.

Signed

Ralph N. Martins (co-author)

Provided funding for the project.

Signed

Michael Lardelli (co-author)

Planned the research and supervised the development of the work. Captured embryo images. Edited the paper prior to submission..

Signed

Abstract and Keywords

Microtubule-associated protein tau (MAPT) is the major component of the neurofibrillary tangles found in the brains of those suffering Alzheimer's disease. Various forms of tau lesion are found in other neurodegenerative diseases (tauopathies). We report identification of two *MAPT* paralogous genes in zebrafish, *mapta* and *maptb*, and analysis of their expression patterns during embryonic development. The two paralogues appear to have arisen by duplication of an ancestral teleost *MAPT* orthologue. Analysis of the splicing of transcripts from both genes during embryogenesis showed that *mapta* can be spliced into isoforms with between four and six tubulin-binding repeats (4R - 6R), while *maptb* is mainly spliced into 3R isoforms. Expression of both genes is observed predominantly in the developing central nervous system. A particularly large isoform of *maptb* is specifically expressed in the trigeminal ganglion and in dorsal sensory neurons of the spinal cord. Changes in the subcellular ratio of 3R and 4R isoforms can have pathological consequences in mammals. The predominant production of 4R-6R isoforms from *mapta* and of 3R isoforms from *maptb* suggests that zebrafish embryos will be a useful tool with which to study the discrete functions and interactions of the 3R and 4R MAPT isoforms.

Keywords: MAPT, tau, zebrafish, Danio rerio, orthologue, embryo, expression, isoform

Introduction

The dysfunction of microtubule-associated protein tau (MAPT) is a major histological characteristic of Alzheimer's disease (AD), and is a common factor in a number of other neurodegenerative disorders including frontotemporal dementia with Parkinson linked to chromosome 17 (FTDP-17), corticobasal degeneration (CBD) and progressive supranuclear palsy (PSP) [1]. In these diseases, collectively known as tauopathies, the normally soluble MAPT proteins aggregate to form lesions in neurons and (for CBD and PSP), also in glial cells. The mechanism of the development of tau lesions is largely unknown and differs among diseases in terms of affected areas and accompanying histological symptoms [1]. However, the consistent presence of insoluble tau aggregations is undoubtedly an important component of these diseases.

Physiologically, the ubiquitously expressed MAPT protein functions as a stabilizer to associate micro-tubules in the human nervous system [2]. A large repertoire of protein isoforms resulting from alternative splicing of *MAPT* transcripts has been identified. However, only six isoforms are most commonly expressed in human brain [3]. These six isoforms can be classified into two groups, referred as 3R or 4R, depending on the number of tubulin-binding motifs (the presence or absence of

exon10 sequence) in their C-termini. Each group contains three isoforms derived from alternative splicing of exon 2 and 3 [3].

The MAPT isoforms are differentially expressed during neuronal development. The shortest isoform is predominantly expressed in human fetus. However, equal levels of 3R and 4R transcripts are found in the adult brains [4]. This precise one-to-one ratio appears to be important to maintaining the physiological function of the MAPT protein, and is altered in most of the neurodegenerative disorders mentioned above in a disease-specific manner [5]. In AD, most early studies failed to find any significant changes in isoform content [6-8]. However, a recent study has suggested that altered splicing occurs in AD-affected brains [9]. In addition to changes in isoform composition, MAPT dysregulation is also characterized by abnormal hyperphosphorylation of the MAPT protein, which detaches MAPT from micro-tubules and leads to the aggregation of the hyperphosphorylated MAPT protein into pretangles, paired helix filaments (PHF), neuropil treads (NTs) or tangles [10]. Much remains unknown about the direct inducers and effectors of tau dysregulation. However, tau dysregulation is correlated with the extensive neuron loss and cognitive decline observed in the relevant neurodegenerative diseases. The intimate participation of MAPT in neurodegenerative disease has been substantiated further by the identification of mutations in *MAPT* as a genetic risk for FTDP-17 [11]. These observations make *MAPT* an interesting gene both in terms of furthering our understanding of the mechanisms underlying these neurodegenerative diseases and as

a potential therapeutic target.

The zebrafish, *Danio rerio,* is an emerging model organism for the study of neurodegenerative disease. Zebrafish embryos can be subjected to subtle and complex manipulation of gene activity. Changes in gene activity can be monitored by observing corresponding changes in the development of their large and easily accessible embryos. Zebrafish embryos bearing mutations in genes orthologous to those involved in human diseases can provide models for dissection of gene function and can be used to screen for therapeutic drugs. In this paper, we report the identification of two *MAPT* paralogous genes in zebrafish, as well as their expression patterns during embryonic development.

Materials and Methods

Phylogenetic and synteny analysis

The conserved regions of MAPT-related protein sequences were aligned using ClustalW (Table 1) with a gap opening penalty of 10 and gap extension penalty of 0.1 for the pairwise alignment stage and a gap opening penalty of 3.0 and gap extension penalty of 1.8 for the multiple alignment stage. The analysis were conducted using PHYML 3.0 [12]. The program was run under the GTR (General Time Reversible) model, with estimated proportion, estimated gamma distribution

parameter, BIONJ input tree and optimized tree topology. The tree reliability was estimated by the approximate Likelihood Ratio Test Method, using SH-like support.

For synteny analysis, the following loci were investigated: in human, region 41.2-59.4M of chromosome 17; in mouse, region 103.6-106.2M of chromosome 11; in chicken, region 1.1-2.9M of chromosome 27; in zebrafish, region 18.9-32.5M of chromosome 3 and region 2.6-20.0M of chromosome 12. The genes contained in the above regions were compared using the Sanger Ensembl and NCBI Entrez Gene databases to identify homologues.

3.2 Cloning of *maptb* and *mapta*

Zebrafish cDNAs were generated from total RNA extracted from whole embryos at 24 hpf and 48 hpf, using Oligo-dT primers as previously described [13]. The *maptb* and *mapta* cDNA fragments were amplified by PCR from 24 hpf cDNA using primers: chr3t (5’-GGACAGACAATAACTCAGTGTGC-3’ and CTTTTCTGGATTCGTCAGTA
GCC-5’) and chr12t (5'-CTATGGACCAGCACCACGATTT-3' and 5’-TCACAAGC
CCTGTTTGG-3’) respectively. The PCR was performed with Dynazyme (FINNZYMES Oy, Espoo, Finland.) at an annealing temperature of 55℃ for 35 cycles. The extension time for the PCR was 2 mins. The PCR fragments were cloned into the pGEM-T vector (Promega) and sequenced.

To confirm the existence of 4R *maptb* isoforms, cDNA fragments were amplified by PCR as above from 24 hpf cDNA using primers: S5 (5'-CATGTTCCTGGTGGTGGTAATG-3') and 3TRR (5'-GATCCAACCTTTGACTGGGCTT-3'); 3TRF (5'-AAGATCGGCTCCACT GAGAACC-3') and R2 (5'- CACATTACCACCACCAGGAACA-3'); 3TRF (5'-A AGATCGGCTCCACTGAGAACC-3') and 3TRR (5'-GATCCAACCTTTGACTGG GCTT-3') (See Figure 3 for primer locations). The PCR product amplified by 3TRF/R2 and S5/3TRR was then sequenced.

To study the coexistence in spliced transcripts of *maptb* exons 3, 5, 9 and 12, the following primers were used to amplify cDNA fragments from 48 hpf cDNA: S1 (5'-TGGGAGCAGAAGCCTTAACACC-3'); S2 (5'-TGGAGACGAGTGATGATGACGA- 3’); S3 (5'-CATGTCCCTTTAGCACTCCAGC-3') ; S4 (5'-CCTGAAAAAAAGGCTGGAGATGC-3') ; S5 (5'-CATGTTCCTGGTGGTGGTAATG-3'); R1 (5'-GACTTAACTAGACTGTTGCCTTC-3'); R2 (5'-CACATTACCACCACCAGGAACA-3'); R3 (5'-CTGGGGATGCCTGTGACTGAAG-3'); R4 （5'-CCAGCCTTTTTTTCAGGAGTTGC-3');

To identify splicing transcript variants of *mapta*, primers that bind regions inside the open reading frame (ORF) were employed. cDNA fragments were amplified from 24 hpf cDNA using the following primers and then sequenced: chr12ts (5'-CTATGGACCAGCACCACGATTT-3'); 12ts' (5'-CTATGGACCAGCACCACGATTT-3'); 12tr' (5'-CCATGTTGATGCTGCCAGAG 3'); 12tas (5'-TCACAAGCCCTGTTTGG-3')

To check the existence of 3R *mapta* isoforms, RT-PCR was performed using primers: 12trf (5'-TCCAAAGTCGGGTCCACTGATA-3') and 12trr (5'-GTTGCCTCCTCCAGGTGTATGT-3'), using 24 hpf and 48 hpf cDNA as templates.

3.3 In situ hybridization

Whole-mount in situ hybridization was conducted according to [14], using single-strand RNA probes labelled with digoxigenin-UTP. The probes were synthesized from *maptb* Variant 2, exon 3 and *mapta* Variant 1 templates.

Double-staining using WISH combined with immunohistochemistry was performed essentially as described by [15], but the WISH staining reagent was BCIP/NBT. The first alkaline phosphatase staining reaction was inactivated by heating at 65°C for 1h in PBT, and the antibody staining reaction used the Alkaline Phosphatase Substrate

Kit I ("Vector Red", Vector Laboratories Inc. Burlingame, CA, USA). zn12[16] antibody was used at a dilution of 1:200.

Results

The identification of zebrafish tau genes via a phylogenetic approach

The *MAPT* gene belongs to the micro-tubule associated protein family. It has been unambiguously recognized in major mammals (e.g., human, mouse and bovine), chickens and frogs. To identify genes with possible orthology to *MAPT* in zebrafish, we searched the NCBI and Ensembl Genome databases using the human MAPT protein sequence.

We found two candidates, previously annotated as “similar to microtubule associated protein tau” in the NCBI database, located on chromosome 3 (XP_001919266) and chromosome 12 (XP_001340566). The E-Values of tBLASTn alignments between these two candidates and human MAPT are similar (1e-96 and 9e-84) and are significantly smaller than other alignments (≥1e-57), which suggests that the two candidates are homologues of human *MAPT*. The amino acid residue identities between human MAPT and the candidates in the conserved C-terminal regions are 62% and 58% respectively (Fig.1.A). To examine the relationship between these candidates and human *MAPT*, we performed a phylogenetic analysis comparing the zebrafish genes with the DNA sequences of MAPT orthologues in human, mouse,

frog, chick, as well as the related proteins MAP2 in human, mouse and frog, and MAP4 in human and mouse (Table.1). The results strongly support that an ancestral *MAPT* orthologue has been duplicated in zebrafish, and that both the candidates are paralogues of human *MAPT* (Fig.1.B).

Analysis of synteny conservation supports the results of the phylogenetic analysis

To support the proposed evolutionary relationship between the two candidates and *MAPT*, neighboring genes on each side of the zebrafish candidate genes were investigated using the Sanger Ensembl database. This led to identification of zebrafish homologues of five genes that are syntenic with human *MAPT* either upstream (LOC587940, *cdc27* and LOC567884) or downstream (*scn4ab* and *nsf*) of the chromosome 3 candidate and homologues of four genes syntenic with human *MAPT* either upstream (LOC564520) or downstream (*scn4aa*, LOC569420 and *nsfb*) of the chromosome 12 candidate. The human orthological relationships of the zebrafish genes *cdc27* [17], *scn4aa*/*scn4ab* [18] and *nsf* [19] have been established previously. tBLASTn searches were performed to confirm that the other neighboring genes of human *MAPT* share highest sequential similarity with their presumptive orthologues in zebrafish (Table. 2). The locations of orthologues of these syntenic genes in mouse and chicken were also identified. Interestingly, the human gene *KIAA1267* and its known or presumptive orthologues in other species exist in a head-to-head orientation with the *MAPT* orthologues in all the species investigated.

In zebrafish, this gene is duplicated and appears upstream of both the chromosome 3 and chromosome 12 *MAPT* candidates (Fig. 2). Thus, analysis of synteny supports that the two candidates are paralogues derived by duplication of an ancestral *MAPT* orthologue. Therefore we have renamed the chromosome 3 and chromosome 12 genes as *maptb* and *mapta* respectively (reflecting the order in which we analysed them).

The structure of *mapta* and *maptb* transcripts

Reverse transcriptase PCR (RT-PCR) was employed to clone cDNAs derived from the mRNAs of zebrafish *mapta* and *maptb*. For *mapta*, we initially identified the existence of four isoforms derived from alternative splicing of exons 8, 9 and 12, using primers 12ts', 12tr' and chr12tas (see Fig. 3A). Inclusion of the 145 bp long exon 12, which follows the last of the exons encoding a tubulin-binding repeat, introduces a stop cordon and truncates the open reading frame (Fig. 3A). Interestingly, exons 8 and 9 also encode tubulin-binding repeats. Thus zebrafish *mapta* can have four, five or six tubulin-binding repeats due to alternative RNA splicing, while human *MAPT* only contains either three or four tubulin-binding repeats. To confirm whether *mapta* can produce an isoform with three tubulin-binding repeats, we performed a RT-PCR test, using primers flanking the entire set of tubulin-binding repeats. This failed to detect any 3R isoform of *mapta* in 24 hpf or 48 hpf embryos (data not shown). The entire ORF of *mapta* was then

amplified and cloned using primer pair chr12ts and chr12tas (Fig. 3A).

For *maptb*, three isoforms resulting from alternative RNA splicing were initially cloned and sequenced using primers targeting regions flanking the entire opening reading frame (ORF) (Fig. 3B,C). Compared to the shortest isoform (splicing Variant 3), splicing Variant 1 of *maptb* includes a 139 bp insert (exon 12) after the tubulin-binding domain in its C-terminal region. Similar to *mapta*, inclusion of this exon truncates the ORF. Splicing Variant 2 of *maptb* includes a 58 amino acid residue insert (exon 5) in its N-terminal region (Fig. 3B).

Interestingly, all of the three isoforms of *maptb* only contains three tubulin-binding repeat motifs in their C-terminal regions, while in adult human brain, approximately equal levels of 3R and 4R *MAPT* isoforms (that include three or four tubulin-binding repeats respectively) are present. We then asked whether the *maptb* gene can generate isoforms with four tubulin-binding motifs. To answer this, we used tBLASTn to search the Sanger Ensembl Genome database, using the sequence of the zebrafish tubulin-binding motif (GSKANIHHKPGGG). A potential exon was found in intron 8 (Fig. 3C). We confirmed the existence of transcripts including this exon by RT-PCR (Fig. 3D). However, the 3R isoforms of *maptb* in 24 hpf and 48 hpf embryos appear to dominate expression, since the 4R transcripts that include this cryptic exon (exon 9) can only be detected when one PCR primer is positioned within it and not when both primers flank the tubulin-binding repeat domain (data

not shown).

The NCBI data based on a combination of ESTs and GNOMON gene-prediction suggested the existence of a 1212 bp exon (exon 3) that can be alternatively spliced in *maptb*. We confirmed the existence of *maptb* isoforms containing this large exon by RT-PCR (Fig. 3C,D), and then sequenced it. To investigate the evolutionary origin of this large exon, we performed a tBLASTn search in the NCBI database. We failed to find any alignments with significant similarity in well-characterised mammals, chicken or frog. The only significant match discovered was to a sequence in salmon, with a putative amino acid residue identity of 37% giving an E-value of 9e-27.

To investigate further the pattern of splicing of *maptb* transcripts, we designed sets of primers for RT-PCR either inside or flanking the four known exons that can be alternatively spliced as indicated by RT-PCR performed above (exons 3, 5, 9 and 12). We showed that all of these exons can co-exist in transcripts (Fig. 3D). This implies the existence of a considerably complex profile of isoform formation for *maptb*.

Expression of zebrafish *mapta*

Using whole mount *in situ* transcript hybridization (WISH), we could first detect *mapta* mRNA at 18 hpf in the telencephalon, ventral diencephalon, caudal floorplate

of the spinal cord and the hypochord (Fig. 4A,C). At 24 hpf, expression increases such that it is discernable in both the ventral and dorsal areas of the telencephalon and in the ventral diencephalon, ventral midbrain and hindbrain rhombomeres (Fig. 4B,D). *mapta* is expressed in a diffuse manner throughout the spinal cord (Fig. 4B). At 48 hpf, expression can be detected in ganglion cells of the retina in addition to the regions described above (Fig. 4F). Meanwhile, expression of *mapta* in the rhombomeres increases and becomes more widespread to form axial to lateral stripes at this stage. The expression in rhombomere 2 is relatively higher than in other rhombomeres (Fig. 4G). The expression of *mapta* in telencephalon, diencephalon and midbrain is also apparently increased at 48 hpf relative to that seen at 24 hpf and begins to be observable in the cerebellum and tectum. However, expression in the spinal cord apparently decreases (Fig. 4H).

1.1 Expression of zebrafish *maptb*

The expression pattern of zebrafish *maptb* partially overlaps that of *mapta*. However, the transcripts of *maptb* are detectable by WISH at an earlier stage as compared to *mapta*. The expression is first evident in the area of the shield at 12 hpf (Fig. 5A). By 18 hpf, relatively weak expression of *maptb* mRNA is detected in the ventral diencephalon, midbrain, rhombomeres (Fig. 5B) and in scattered neurons of the dorsal spinal cord (Fig. 5B). In contrast, relatively much higher expression of *maptb*

mRNA is observed in the developing trigeminal ganglion, which is located lateral and somewhat caudal to the midbrain-hindbrain boundary (Fig. 5B,C). At 24 hpf, the expression of *maptb* mRNA increases and can be observed in ventral telencephalon in addition to the above regions (Fig. 5E). To understand better the expression domain of *maptb*, we double-labeled 27 hpf embryos using the monoclonal antibody zn12 and WISH for *maptb*. This confirmed expression of *maptb* in the trigeminal ganglion (Fig. 5H,I,N) and showed that *maptb* is expressed in Rohon-Beard neurons (Fig. 5D,F). Notably, however, *mapta* expression is not observed in these two regions. At 48 hpf, expression of *maptb* in brain continues in similar regions as observed at 24 hpf, however, the level of expression appears to be increased (Fig. 5O). Compared to younger embryos, expression in the telencephalon and diencephalon has expanded in these domains. However, the telencephalon-diencephalon boundary remains visible through its lack of expression (Fig. 5O). Expression in the hindbrain also becomes more extensive to form an axial to lateral band in each rhombomere (Fig. 5M) that, nevertheless, is restricted to the ventral half of the hindbrain. In addition, expression of *maptb* is evident in the cerebellum (Fig. 5M). In the spinal cord, *maptb*-expressing neurons show highest expression in more caudal regions (Fig. 5O).

Our study of *maptb* mRNA isoforms showed the existence of a particularly long *maptb* transcript containing an additional 1212 bp exon. Using a riboprobe specific for this exon we could investigate the expression pattern of this “big” isoform by WISH. This showed expression of the big isoform in the trigeminal ganglia and

dorsal spinal cord neurons. No expression was detected in the telencephalon, diencephalon and hindbrain in embryos at 18 hpf and 24 hpf (Fig. 6). However, relatively much weaker expression in the rostral ventral diencephalon and hindbrain can be detected at 48 hpf by extended staining.

Discussion

The *MAPT* gene has attracted extensive interest due to its critical role in the development of various neurodegenerative diseases. To achieve a better understanding of *MAPT* function and dysfunction, multiple animal models have been employed [20]. The zebrafish and its embryos have been demonstrated to be a highly tractable vertebrate model for genetic studies due to a beneficial combination of characteristics including easy embryo accessibility, large embryo size, rapid embryonic development, short generation time and a well-characterised genome [21]. Indeed, transgenic zebrafish expressing human *MAPT* have previously been used to investigate MAPT pathology [22, 23]. However, the zebrafish endogenous *MAPT* gene has not been characterized. Here we identified two *MAPT* paralogues (*mapta* and *maptb*) in zebrafish via a combination of phylogenetic and conserved synteny analysis. These are apparently derived from a duplication of an ancestral teleost *MAPT* orthologue. Alignments between human MAPT and the zebrafish genes show high conservation in the tubulin-binding domain and the C-terminal tail of the gene. This is the region providing major affinity for MAPT proteins to bind microtubules.

The N-terminus of MAPT protein is a “projection domain”, which interacts with the axonal membrane [24]. After that is a “hinge region” functioning as a spacer to determine the distance between microtubules in microtubule bundles [25]. In these two regions the amino acid residue sequences of human MAPT and the putative zebrafish proteins do not show conservation. Furthermore, even the two zebrafish *MAPT* paralogues show low similarity in the N-terminal half, indicating lower selective pressure for sequence conservation of this region or, alternatively, divergent selective pressures on the two paralogues.

The splicing of transcripts from human *MAPT* shows complex regulation. Of the known 16 exons of human tau, eight (2, 3, 4A, 6, 8, 10, 13, 14) show alternatively splicing [3]. Six tau isoforms (derived from alternative splicing of exons 2, 3 and 10) are the major isoforms observed in human brain [26]. The duplicated *MAPT* paralogues in zebrafish show similar complexity of alternative splicing. For *maptb*, at least four exons can be spliced alternatively. Our RT-PCR results show that all of the four exons can coexist in transcripts, indicating the existence of a considerable number of splicing isoforms. Interestingly, the *maptb* gene encodes a particularly large exon (exon 3) that can be alternatively spliced into the N-terminal half of the open reading frame. Inclusion of this exon almost doubles the length of the *maptb* open reading frame. This is reminiscent of the “big tau” isoform (isoform 6) in humans which also contains a relatively large exon (exon 4A) in its N-terminal region and is specifically expressed in retina and peripheral nervous system [3].

However, blast analysis showed no significant sequence homology between exon 4A of human “big tau” and zebrafish *maptb* exon 3. In fact, a tBLASTn search in the NCBI nonredundant database failed to find any significant homologies between *maptb* exon 3 and sequences in mammals, amphibians and birds.

Alternative splicing of exon 2 and exon 3 of human *MAPT* produces three protein isoforms with inserts of 0, 29 or 58 amino acid residues in their N-terminal halves [26]. Similarly, zebrafish *maptb* possesses an exon encoding a putative 58 amino acid residues (exon5) and this can be alternatively spliced. However, this exon shares no significant sequence similarity with exon 2 or exon 3 of human *MAPT* and it is located after the large exon. Therefore it remains obscure whether exon 5 of *maptb* serves a similar function to exon 2 and 3 of human *MAPT*.

The precise regulation of the ratio of expression of 3R relative to 4R *MAPT* isoforms has been proposed to be critical for maintaining normal brain function [27]. The disruption of this balance has been found to be correlated with tauopathies [27]. Furthermore, most FTD-associated *MAPT* mutations alter the level of 3R and 4R *MAPT* isoforms [28]. Therefore, the tubulin-binding domain plays a significant role in the regulation of MAPT function. Our initial RT-PCR results indicated that *maptb* might only encode three tubulin-binding repeats. Later, we identified an additional exon encoding a tubulin-binding repeat by a BLAST search of the zebrafish genome sequence. We confirmed the inclusion of this exon in spliced *matpb* transcripts by

RT-PCR. In mouse, 3R *Mapt* is predominately expressed during embryo development. The 4R isoforms begin to increase by postpartum day 6 (P6) and become the predominant isoforms by P24 [29]. However in zebrafish, the level of 4R transcripts produced from *maptb* is still relatively very low by 48 hpf (when hatching can begin). On the other hand, we failed to detect any 3R isoforms from the *mapta* gene by RT-PCR using primers flanking the tubulin-binding domain. Although this does not exclude the possibility of the existence of trace levels of 3R transcript isoforms from *mapta*, the major *mapta* transcript products appear to contain four to six tubulin-binding motifs in 24 hpf and 48 hpf embryos. *In vitro* studies showed that the presence of the fourth tubulin-binding motif in human MAPT almost triples the affinity between MAPT protein and microtubules [30, 31]. Therefore, the inclusion of two additional tubulin-binding motifs may increase the efficiency of Mapta protein in stabilization of microtubules.

Whole-mount *in situ* transcript hybridisation showed that mRNA from *maptb* can be detected earlier than that from *mapta*. This is not surprising, given that *MAPT* 3R isoforms are predominant in both human and mouse fetal stages. The expression of *maptb* also appears relatively stronger than *mapta* in 18 hpf and 24 hpf embryos (judging by the speed of colour development during staining although this can be highly variable and dependent on multiple factors such as embryo batch, fixation time, probe quality, etc.). However, at the 48 hpf stage, the expression level of *maptb* and *mapta* appeared to be more similar. Moreover, *mapta* expression became more

spatially extensive compared to *maptb* covering almost the entire brain region at this stage.

By WISH, we showed that *maptb* mRNA that includes the large exon 3 is expressed mainly in the trigeminal ganglion and dorsal spinal cord neurons at 24 hpf and 48 hpf. Apart from the observation of very weak expression in anterior ventral diencephalon and hindbrain in 48 hpf embryos after extended straining, the mRNA of this putative zebrafish “big tau” was undetectable in the brain. This coincides with the expression pattern of rat “big tau”, which is specifically expressed in the peripheral nervous system [32, 33]. Therefore, although the large exon 3 of zebrafish *maptb* “big tau” shares no detectable similarity with that of mammalian “big tau” at the amino acid sequence level, their expression patterns appear related, indicating possible conservation of function.

In mice, *Mapt* expression begins at the E10.0 stage. Expression is detected in brain, retina, spinal cord, and testis, which is consistent with what we observe for *mapta* and *maptb* in zebrafish. The similar expression pattern of *Mapt* in the two species indicates conserved function during evolution. Therefore, zebrafish can be a practical model for study of MAPT and its roles in human neurodegenerative diseases.

The expression patterns of *mapta* and *maptb* appear similar in the central nervous

system. However, the following differences between the two paralogues were noted: First, *maptb* is expressed in Rohon-Beard neurons while *mapta* is expressed in the floorplate and caudal hypochord. In addition, *mapta* expresses in a diffuse manner in the developing spinal chord, while *maptb* expression is restricted to Rohon-Beard neurons. At 48 hpf, the expression of *mapta* in the spinal cord decreased dramatically compared to younger embryos. The expression of *maptb* in spinal cord neurons also appeared to show a certain level of decrease and became restricted to more caudal regions compared to that in 24 hpf embryos. Second, *mapta* but not *maptb* mRNA is detectable in ganglion neurons of the retina. Third, at 48 hpf, the expression of *mapta* in brain increases and covers a broader region relative to *maptb*, including the tectum and the dorsal half of the hindbrain. The different expression patterns of *mapta* and *maptb* in some regions indicate probable subfunctionalisation of the role of an ancestral *MAPT* orthologue after their formation by duplication. This subfunctionalisation may have been enhanced by the changes in the number of tubulin-binding repeats that each gene encodes. Therefore, future study of the functional difference between *mapta* and *maptb* may tell us more about how the number of tubulin-binding motifs modifies vertebrate *MAPT* function.

Acknowledgments including sources of support

This work was supported by a Project Grant (453622) to M. Lardelli and R.N. Martins from the National Health and Medical Research Council of Australia.

Animal experimentation was carried out under the auspices of the Animal Ethics Committee of the University of Adelaide.

References

[1] Pittman AM, Fung HC, de Silva R (2006) Untangling the tau gene association with neurodegenerative disorders. *Hum Mol Genet* **15 Spec No 2**, R188-195.

[2] Wang JZ, Liu F (2008) Microtubule-associated protein tau in development, degeneration and protection of neurons. *Prog Neurobiol* **85**, 148-175.

[3] Andreadis A (2005) Tau gene alternative splicing: expression patterns, regulation and modulation of function in normal brain and neurodegenerative diseases. *Biochim Biophys Acta* **1739**, 91-103.

[4] Rademakers R, Cruts M, van Broeckhoven C (2004) The role of tau (MAPT) in frontotemporal dementia and related tauopathies. *Hum Mutat* **24**, 277-295.

[5] Goedert M, Spillantini MG (2006) A century of Alzheimer's disease. *Science* **314**, 777-781.

[6] Connell JW, Rodriguez-Martin T, Gibb GM, Kahn NM, Grierson AJ, Hanger DP, Revesz T, Lantos PL, Anderton BH, Gallo JM (2005) Quantitative analysis of tau isoform transcripts in sporadic tauopathies. *Brain Res Mol Brain Res* **137**, 104-109.

[7] Boutajangout A, Boom A, Leroy K, Brion JP (2004) Expression of tau mRNA and soluble tau isoforms in affected and non-affected brain areas in Alzheimer's disease. *FEBS Lett* **576**, 183-189.

[8] Ingelsson M, Ramasamy K, Cantuti-Castelvetri I, Skoglund L, Matsui T, Orne J, Kowa H, Raju S, Vanderburg CR, Augustinack JC, de Silva R, Lees AJ, Lannfelt L, Growdon JH, Frosch MP, Standaert DG, Irizarry MC, Hyman BT (2006) No alteration in tau exon 10 alternative splicing in tangle-bearing neurons of the Alzheimer's disease brain. *Acta Neuropathol* **112**, 439-449.

[9] Conrad C, Zhu J, Conrad C, Schoenfeld D, Fang Z, Ingelsson M, Stamm S, Church G, Hyman BT (2007) Single molecule profiling of tau gene expression in Alzheimer's disease. *J Neurochem* **103**, 1228-1236.

[10] Ballatore C, Lee VM, Trojanowski JQ (2007) Tau-mediated neurodegeneration in Alzheimer's disease and related disorders. *Nat Rev Neurosci* **8**, 663-672.

[11] Goedert M, Jakes R (2005) Mutations causing neurodegenerative tauopathies. *Biochim Biophys Acta* **1739**, 240-250.

[12] Guindon S, Gascuel O (2003) A simple, fast, and accurate algorithm to estimate large phylogenies by maximum likelihood. *Syst Biol* **52**, 696-704.

[13] Nornes S, Groth C, Camp E, Ey P, Lardelli M (2003) Developmental control of Presenilin1 expression, endoproteolysis, and interaction in zebrafish embryos. *Exp Cell Res* **289**, 124-132.

[14] Tamme R, Mills K, Rainbird B, Nornes S, Lardelli M (2001) Simple, directional cDNA cloning for in situ transcript hybridization screens. *Biotechniques* **31**, 938-942, 944, 946.

[15] Jowett T (1997) *Tissue in situ hybridization*, John Wiley & Sons, New York.

[16] Trevarrow B, Marks DL, Kimmel CB (1990) Organization of hindbrain segments in the zebrafish embryo. *Neuron* **4**, 669-679.

[17] Gates MA, Kim L, Egan ES, Cardozo T, Sirotkin HI, Dougan ST, Lashkari D, Abagyan R, Schier AF, Talbot WS (1999) A genetic linkage map for zebrafish: comparative analysis and localization of genes and expressed sequences. *Genome Res* **9**, 334-347.

[18] Novak AE, Jost MC, Lu Y, Taylor AD, Zakon HH, Ribera AB (2006) Gene duplications and evolution of vertebrate voltage-gated sodium channels. *J Mol Evol* **63**, 208-221.

[19] Woods IG, Lyons DA, Voas MG, Pogoda HM, Talbot WS (2006) nsf is essential for organization of myelinated axons in zebrafish. *Curr Biol* **16**, 636-648.

[20] Stoothoff WH, Johnson GV (2005) Tau phosphorylation: physiological and pathological consequences. *Biochim Biophys Acta* **1739**, 280-297.

[21] Newman M, Musgrave IF, Lardelli M (2007) Alzheimer disease: amyloidogenesis, the presenilins and animal models. *Biochim Biophys Acta* **1772**, 285-297.

[22] Tomasiewicz HG, Flaherty DB, Soria JP, Wood JG (2002) Transgenic zebrafish model of neurodegeneration. *J Neurosci Res* **70**, 734-745.

[23] Bai Q, Garver JA, Hukriede NA, Burton EA (2007) Generation of a transgenic zebrafish model of Tauopathy using a novel promoter element derived from the zebrafish eno2 gene. *Nucleic Acids Res* **35**, 6501-6516.

[24] Brandt R, Leger J, Lee G (1995) Interaction of tau with the neural plasma membrane mediated by tau's amino-terminal projection domain. *J Cell Biol* **131**, 1327-1340.

[25] Chen J, Kanai Y, Cowan NJ, Hirokawa N (1992) Projection domains of MAP2 and tau determine spacings between microtubules in dendrites and axons. *Nature* **360**, 674-677.

[26] Dermaut B, Kumar-Singh S, Rademakers R, Theuns J, Cruts M, Van Broeckhoven C (2005) Tau is central in the genetic Alzheimer-frontotemporal dementia spectrum. *Trends Genet* **21**,

664-672.

[27] Brandt R, Hundelt M, Shahani N (2005) Tau alteration and neuronal degeneration in tauopathies: mechanisms and models. *Biochim Biophys Acta* **1739**, 331-354.

[28] Kar A, Kuo D, He R, Zhou J, Wu JY (2005) Tau alternative splicing and frontotemporal dementia. *Alzheimer Dis Assoc Disord* **19 Suppl 1**, S29-36.

[29] McMillan P, Korvatska E, Poorkaj P, Evstafjeva Z, Robinson L, Greenup L, Leverenz J, Schellenberg GD, D'Souza I (2008) Tau isoform regulation is region- and cell-specific in mouse brain. *J Comp Neurol* **511**, 788-803.

[30] Butner KA, Kirschner MW (1991) Tau protein binds to microtubules through a flexible array of distributed weak sites. *J Cell Biol* **115**, 717-730.

[31] Goode BL, Chau M, Denis PE, Feinstein SC (2000) Structural and functional differences between 3-repeat and 4-repeat tau isoforms. Implications for normal tau function and the onset of neurodegenetative disease. *J Biol Chem* **275**, 38182-38189.

[32] Georgieff IS, Liem RK, Mellado W, Nunez J, Shelanski ML (1991) High molecular weight tau: preferential localization in the peripheral nervous system. *J Cell Sci* **100 (Pt 1)**, 55-60.

[33] Goedert M, Spillantini MG, Crowther RA (1992) Cloning of a big tau microtubule-associated protein characteristic of the peripheral nervous system. *Proc Natl Acad Sci U S A* **89**, 1983-1987.

Tables

Table. 1. Sequences used in the phylogenetic analysis

Common Name	**Species Name**	**Sequence**	**Sequence Accession Numbers**
Zebrafish	*Danio rerio*	Loc100000342	XM_001340530
		Loc567833	XM_001919231
Human	*Homo sapiens*	MAPT	NM_005910
		MAP2	NM_031847
		MAP4	NM_030884
Mouse	*Mus musculus*	Mapt	NM_001038609
		Mtap2	NM_001039934
		Mtap4	NM_008633
Frog	*Xenopus tropicalis*	mapt	NM_001078997
		map2	NM_001079120
Chicken	*Gallus gallus*	MAPT	XM_424354

Table.2 Summary of tBLASTn search results in the analysis of synteny conservation. Maximum quality hits are shown in descending order. Loci presumably orthologous to the probe sequences are indicated by grey shading (including "duplicate orthologues").

Probe	Traget organism	Hits	Quality (E-value)	Probe	Traget organism	Hits	Quality (E-value)
Human *KIAA1267*	zebrafish	LOC567884	0.0	Zebrafish LOC567884	human	*KIAA1267*	0.0
		LOC564520	1.0e-173			*C2orf67*	5.0e-19
		LOC561374	1.0e-27	zebrafish LOC564520	human	*KIAA1267*	3.0e-170
						C2orf67	2.0e-19
Human *CRHR1*	zebrafish	LOC567940	0.0	zebrafish LOC558175	human	*CRHR2*	1.0e-154
		LOC558175	2.0e-139			*CRHR1*	4.0e-139
Human *Wnt3*	zebrafish	*wnt3*	0.0	zebrafish *wnt31*	human	*WNT3A*	0.0
		wnt31	0.0			*WNT3*	0.0
		LOC100148792	2.0e-89				
Human *NSF*	zebrafish	*nsf*	0.0	zebrafish *nsfb*	human	*NSF*	0.0
		nsfb	0.0			LOC728806	0.0
		327197 vcp	3.0e-46				

Figure Legends

Fig.1. (A) Amino acid residue sequence alignment of the two zebrafish MAPT candidates and human MAPT performed using ClustalX2.0.5. with default parameters. Only the conserved region is shown. Black shading indicates identical residues and grey shading indicates similar residues. (B) Maximum likelihood tree of the microtubule-associated protein family generated using PHYML3.0. Numbers represent the aLRT branch-support values. Sequences used in the phylogenetic analysis are shown in Table 1.

Fig.2. Schematic showing genes syntenic with the presumptive zebrafish *MAPT* paralogues and human (*Hs*), mouse *(Mm)*, and chicken (*Gg*) *MAPT* genes. The loci of these genes are shown on the numbered horizontal line. Arrows indicate direction of gene transcription. The table shows homology relationships between genes in different organisms.

Fig.3. Splicing isoforms of *mapta* and *maptb* mRNA transcripts. Light blue and red boxes indicate exons that can be alternatively spliced. The light red boxes indicate exons encoding tubulin-binding motifs. Arrows in the grey area indicate the approximate binding sites of primers used in RT-PCR analysis of splicing isoforms. (A) Exon structure of *mapta*. (B) Structure of three identified *maptb* transcript isoforms. White boxes indicate exons absent in these transcripts. (C) Exon structure

of *maptb*. Primers S4 and R4 span the exon4/exon6 fusion boundary. (D) Gel electrophoresis of RT-PCR products demonstrating the co-existence in transcripts of particular exons. NPPO stands for “no PCR production observed”.

Fig.3. (black/white) Splicing isoforms of *mapta* and *maptb* mRNA transcripts. Grey and striped boxes indicate exons that can be alternatively spliced. The striped boxes indicate exons encoding tubulin-binding motifs. Arrows in the grey areas indicate the approximate binding sites of primers used in RT-PCR analysis of splicing isoforms. (A) Exon structure of *mapta*. (B) Structure of three identified *maptb* transcript isoforms. White boxes indicate exons absent in these transcripts. (C) Exon structure of *maptb*. Primers S4 and R4 span the exon4/exon6 fusion boundary. (D) Gel electrophoresis of RT-PCR products demonstrating the co-existence in transcripts of particular exons. NPPO stands for “no PCR production observed”.

Fig.4 Expression of *mapta* during embryogenesis as detected by WISH. Rostral is to the left and dorsal is up unless otherwise indicated. (A, C) Expression at 18 hpf. (A) Lateral view showing weak expression in the telencephalon. (C) Transverse optical view of an 18 hpf embryo at a position indicated in A by the line labeled with “C”. Expression is evident in floorplate (upper) and hypocord (lower) areas. (B, D, E) Expression at 24 hpf. (B) Lateral view showing expression in the telencephalon, diencephalon and midbrain. *mapta* is expressed in the floorplate and diffusely throughout the remainder of the spinal cord. Arrowhead indicates expression in the

chordoneural hinge area. (D) Dorsal axial view of an embryo with yolk removed. Expression is highest in the telencephalon but is also seen in rhombomeres. (E) Transverse optical section in the region of the yolk extension showing the diffuse expression in the spinal cord. (F-H) Expression at 48 hpf. (F) Optical section through the eye. Expression of *mapta* is observed in ganglion cells of the retina (arrowhead). (G) Dorsal axial view of the hindbrain. Expression is strongest in rhombomere 2. (H) Lateral view showing that expression is predominantly in the brain. Size bars indicate 100μm. *Abbrevations:* dc, diencephalon; fp, floor plate; hb, hindbrain; hc, hypochord; mb, midbrain; ot, otic vesicle; nc, notochord; r2, 3, 4, 5, rhombomere 2, 3, 3, 5; sc, spinal cord; tc, telencephalon;

Fig.5. Expression pattern of *maptb* mRNA during embryogenesis as detected by WISH. Rostral is always to the left and dorsal is up unless otherwise indicated. (A) A lateral view (animal pole to top) at 6 hpf shows expression in the shield. (B-C) Expression at 18 hpf (B) Lateral view showing expression in ventral diencephalon, midbrain, rhombomeres, trigeminal ganglion (see boxed area) and dorsal spinal cord neurons. (C) Dorsal axial view showing expression in trigeminal ganglia and rhombomeres. (D-I, N) Expression at 24 hpf. (E) Lateral view, arrowhead indicates expression in trigeminal ganglion. (G) Dorsal axial view of a flat mounted embryo with yolk removed. Arrowheads indicate expression in trigeminal ganglia. (C, D, F, H, I, N) Embryos doubly-labelled to show *maptb* mRNA (blue) and the zn12 antibody antigen (red) at 27 hpf. (F) Lateral view, arrowheads denote rostral

Rohon-Beard neurons. (D) Dorsolateral view, with arrowheads indicating similar cells to those in F. (H) Dorsal axial view, showing co-expression of *maptb* and zn12 antigen in trigeminal ganglia. (I, N) Different magnifications of an image showing *maptb* mRNA in a subset of the cells of the trigeminal ganglion. (J-M, O) Expression at 48 hpf. (J) Lateral view of the head. Arrowhead indicates expression in trigeminal ganglion. (K) Dorsolateral view with arrow indicating expression caudal to the otic vesicle. (M) Dorsal axial view showing expression in cerebellum and rhombomeres. (O) Lateral view of entire embryo. Expression is predominantly in the brain. Size bars indicate 100μm. *Abbrevations:* dc, diencephalon; hb, hindbrain; mb, midbrain; ot, otic vesicle; r2, 3, 4, 5, rhombosmere 2, 3, 4, 5; tc, telencephalon; tg, trigeminal ganglion.

Fig.6 Expression of *maptb* isoforms that include the 1212 bp exon 3. (A) Lateral view of a 24 hpf embryo. Expression is observed predominantly in trigeminal ganglia and spinal cord neurons. (B) Dorsal axial view, showing expression in trigeminal ganglia lateral to the midbrain-hindbrain boundary. Size bars indicate 100μm. *Abbrevations:* hb, hindbrain; mb, midbrain.

Fig.1.

A

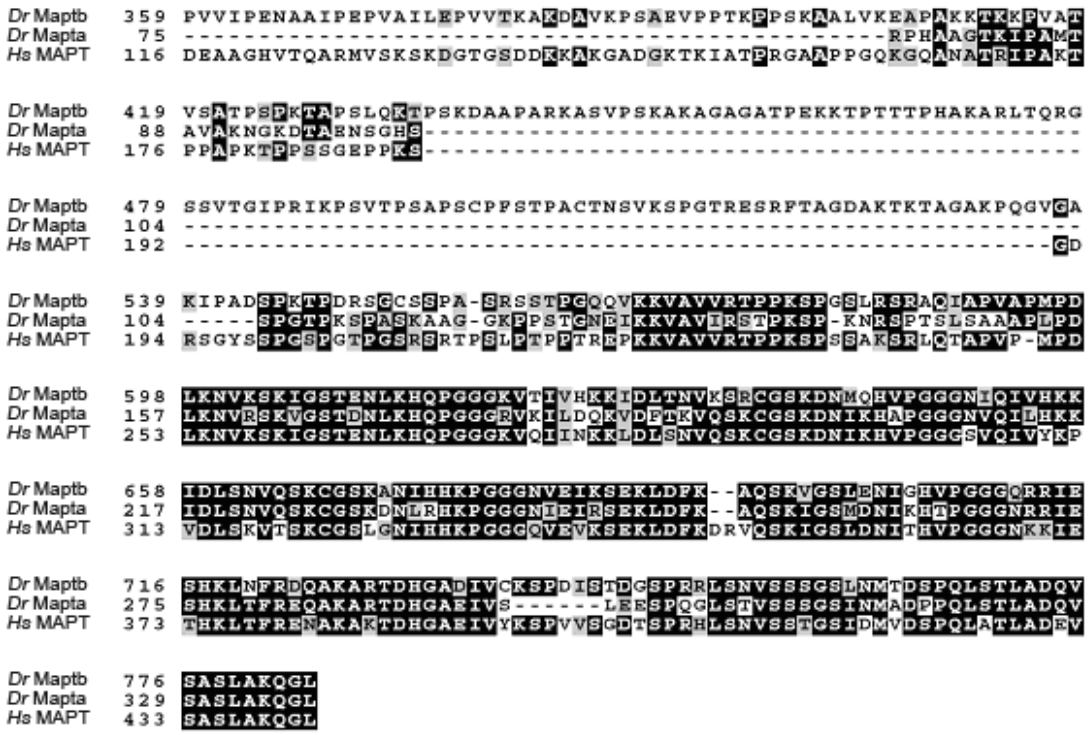
Dr Maptb 359 PVVIPENAAIPEPVAILEPVVTKAKDAVKPSAEVPPTKPPSKAALVKEAPAKKTKKPVAT
Dr Mapta 75 ----------RPHAAGTKIPAMT
Hs MAPT 116 DEAAGHVTQARMVSKSKDGTGSDDKKAKGADGKTKIATPRGAAPPGQKGQANATRIPAKT
Dr Maptb 419 VSATPSPKTAPSLQKTPSKDAAPARKASVPSKAKAGAGATPEKKTPTTTPHAKARLTQRG
Dr Mapta 88 AVAKNGKDTAENSGHS----------
Hs MAPT 176 PPAPKTPPSSGEPPKS----------
Dr Maptb 479 SSVTGIPRIKPSVTPSAPSCPFSTPACTNSVKSPGTRESRFTAGDAKTKTAGAKPQGVGA
Dr Mapta 104 ----------
Hs MAPT 192 ----------GD
Dr Maptb 539 KIPADSPKTPDRSGCSSPA-SRSSTPGQQVKKVAVVRTPPKSPGSLRSRAQIAPVAPMPD
Dr Mapta 104 -----SPGTPKSPASKAAG-GKPPSTGNEIKKVAVIRSTPKSP-KNRSPTSLSAAAPLPD
Hs MAPT 194 RSGYSSPGSPGTPGSRSRTPSLPTPPTREPKKVAVVRTPPKSPSSAKSRLQTAPVP-MPD
Dr Maptb 598 LKNVKSKIGSTENLKHQPGGGKVTIVHKKIDLTNVKSRCGSKDNMQHVPGGGNIQIVHKK
Dr Mapta 157 LKNVRSKVGSTDNLKHQPGGGRVKILDQKVDFTKVQSKCGSKDNIKHAPGGGNVQILHKK
Hs MAPT 253 LKNVKSKIGSTENLKHQPGGGKVQIINKKLDLSNVQSKCGSKDNIKHVPGGGSVQIVYKP
Dr Maptb 658 IDLSNVQSKCGSKANIHHKPGGGNVEIKSEKLDFK--AQSKVGSLENIGHVPGGGQRRIE
Dr Mapta 217 IDLSNVQSKCGSKDNLRHKPGGGNIEIRSEKLDFK--AQSKIGSMDNIKHTPGGGNRRIE
Hs MAPT 313 VDLSKVTSKCGSLGNIHHKPGGGQVEVKSEKLDFKDRVQSKIGSLDNITHVPGGGNKKIE
Dr Maptb 716 SHKLNFRDQAKARTDHGADIVCKSPDISTDGSPRRLSNVSSSGSLNMTDSPQLSTLADQV
Dr Mapta 275 SHKLTFREQAKARTDHGAEIVS------LEESPQGLSTVSSSGSINMADPPQLSTLADQV
Hs MAPT 373 THKLTFRENAKAKTDHGAEIVYKSPVVSGDTSPRHLSNVSSTGSIDMVDSPQLATLADEV
Dr Maptb 776 SASLAKQGL
Dr Mapta 329 SASLAKQGL
Hs MAPT 433 SASLAKQGL

B

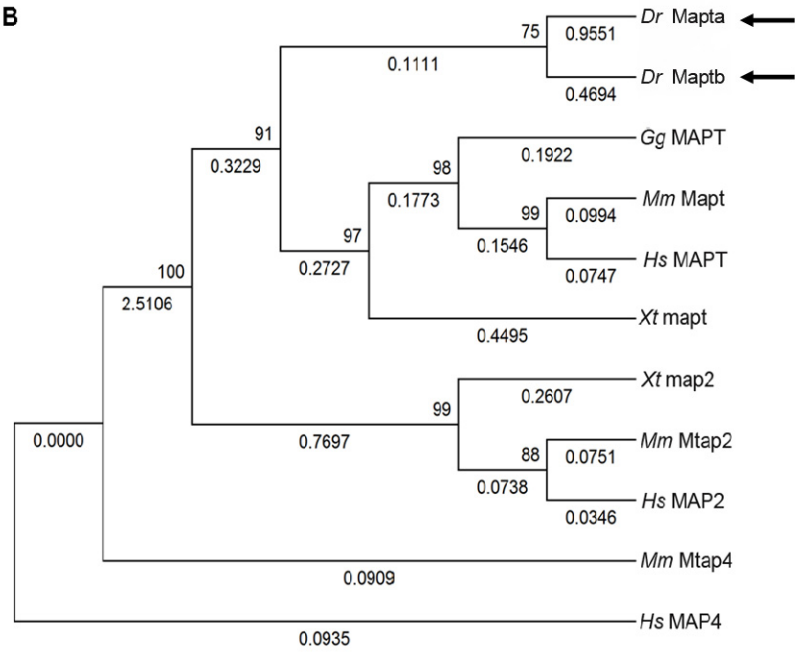
Dr Mapta
Dr Maptb
Gg MAPT
Mm Mapt
Hs MAPT
Xt mapt
Xt map2
Mm Mtap2
Hs MAP2
Mm Mtap4
Hs MAP4
75
0.9551
0.1111
0.4694
91
0.3229
98
0.1922
0.1773
99
0.0994
97
0.1546
0.2727
0.0747
100
2.5106
0.4495
0.2607
99
0.0000
0.7697
88
0.0751
0.0738
0.0346
0.0909
0.0935

Fig.2.

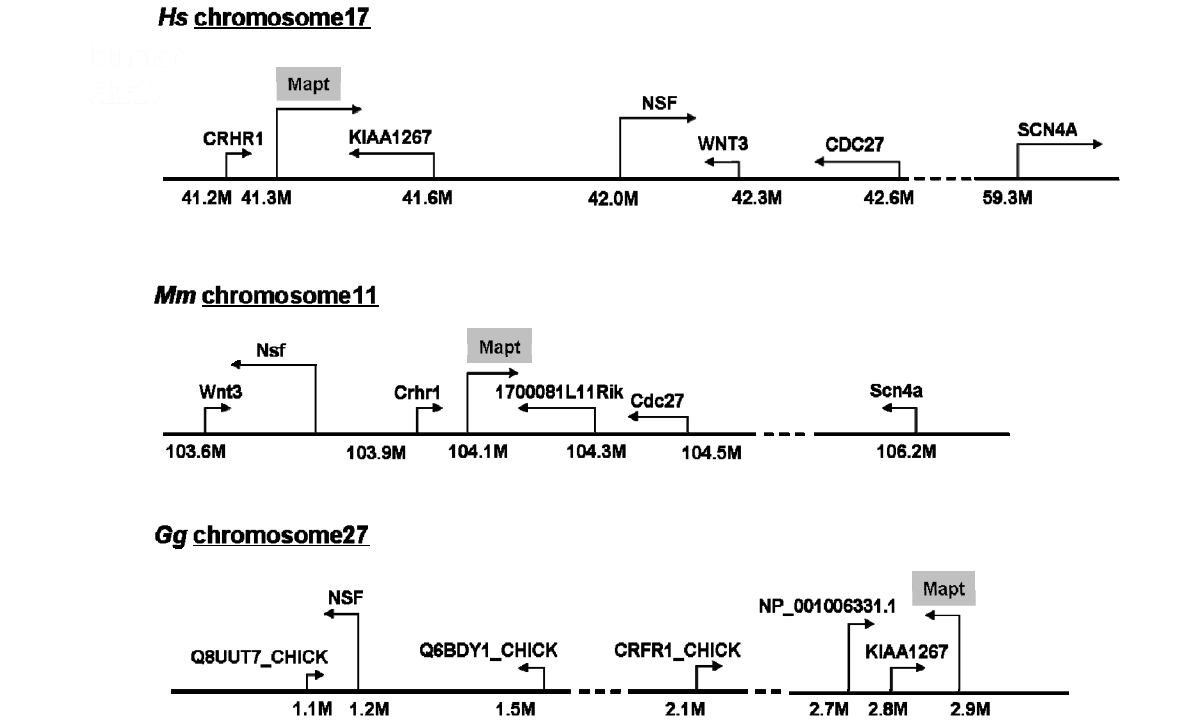

Homologue matches

Hs	*Mm*	*Gg*	*Dr*
Mapt	*Mapt*	*Mapt*	*mapta* *maptb*
CRHR1	*Crhr1*	*CRFR1_CHICK*	LOC567940
KIAA1267	*1700081L11Rik*	*KIAA1267*	LOC567884 LOC564520
NSF	*Nsf*	*NSF*	*nsf* *nsfb*
WNT3	*Wnt3*	*Q8UUT7_CHICK*	LOC569420
CDC27	*Cdc27*	*NP_001006331.1*	*cdc27*
SCN4A	*Scn4a*	*Q6BDY1_CHICK*	*scn4aa* *scn4ab*

Fig.3.

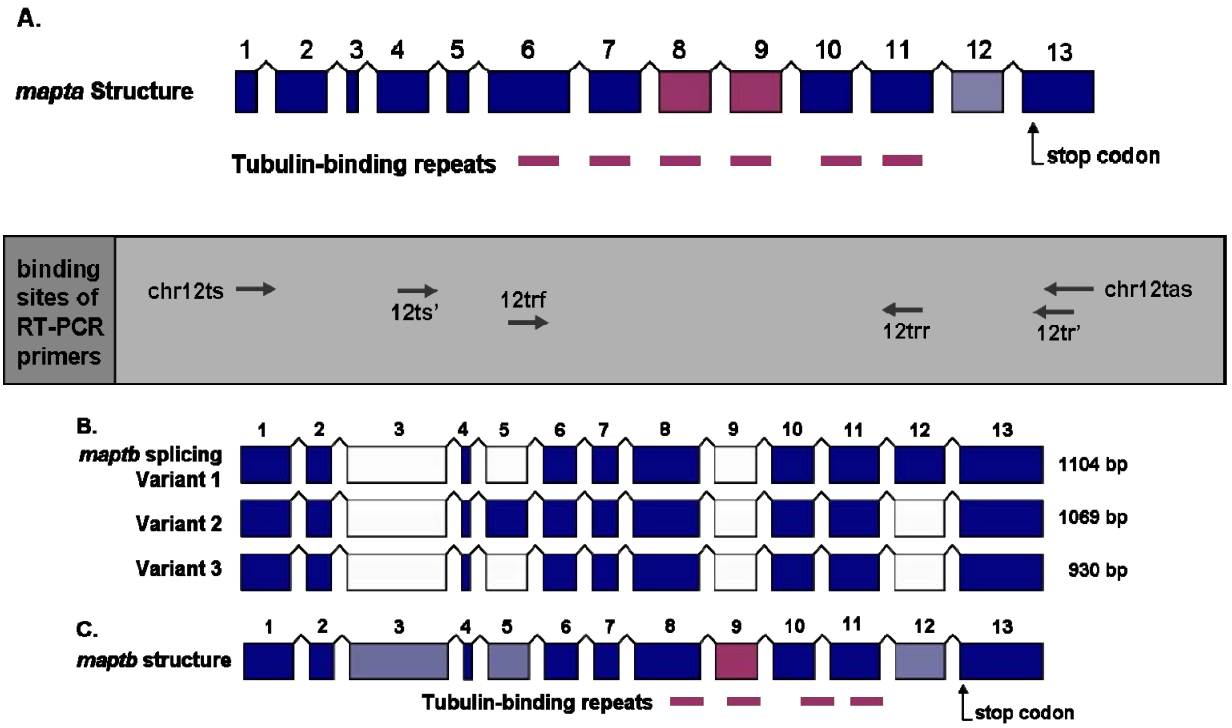

D.

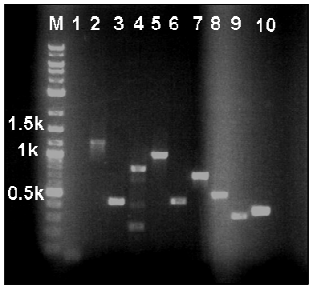

Tests of exon co-inclusion in transcripts by RT-PCR

Gel lane	Primer pair	Exons	Predicted size (bp)	Gel lane	Primer pair	Exons	Predicted size (bp)
1	S1/R3	NPPO	1324	6	S4/R2	E4-E6-E9	456
2	S1/R4	E3-E4-E6	1258	7	S3/R1	E5-E12 (E9X)	736
3	S2/R3	E3-E4-E5	445	8	S3/R2	E5-E9	515
4	S2/R2	E3-E9 (E5X)	818	9	S5/R1	E9-E12	339
5	S2/R1	E3-E12 (E5X, E9X)	1039	10	S2/R4	E3-E4-E6	379

Fig. 3 black/white version

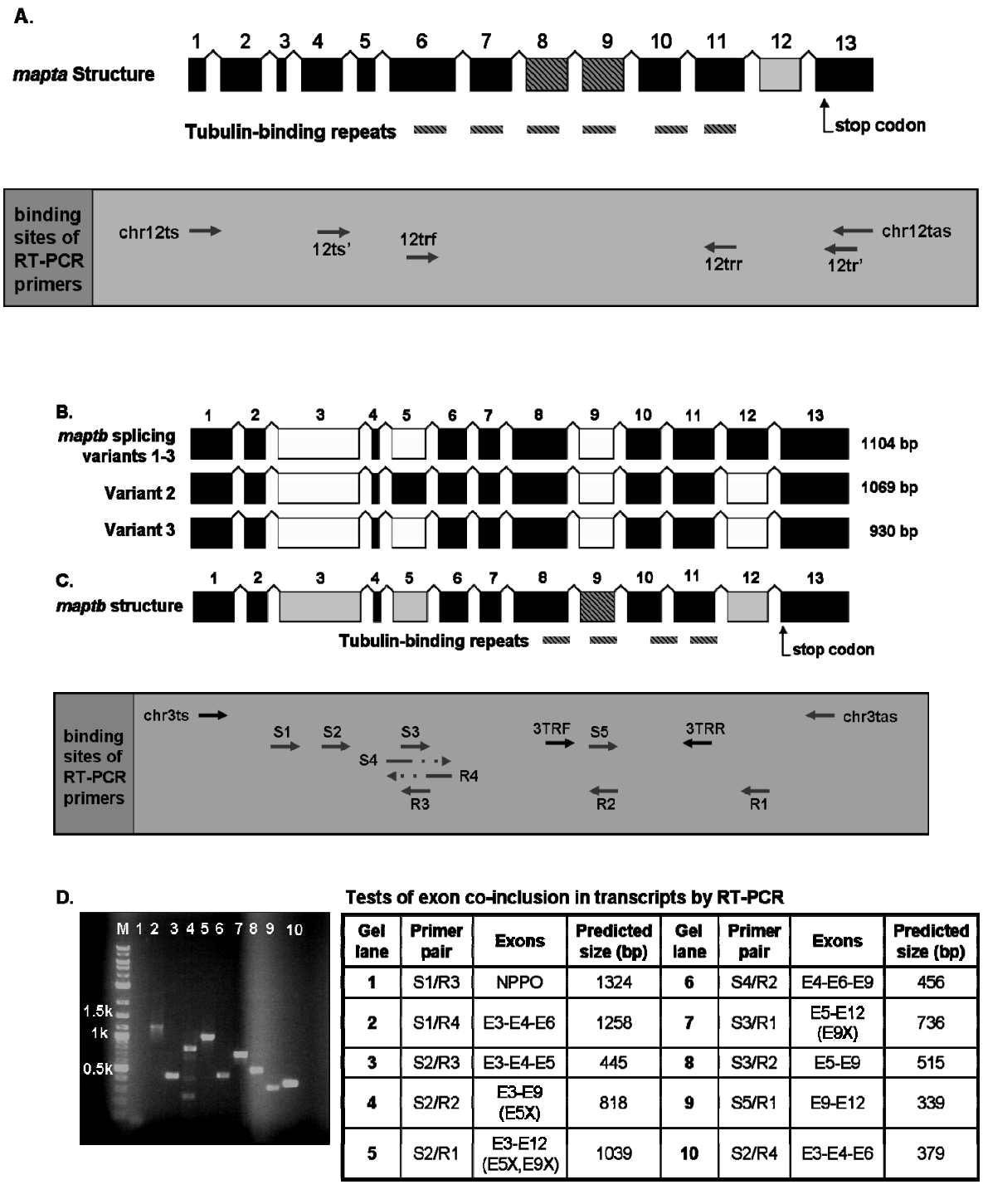

D.

Tests of exon co-inclusion in transcripts by RT-PCR

Gel lane	Primer pair	Exons	Predicted size (bp)	Gel lane	Primer pair	Exons	Predicted size (bp)
1	S1/R3	NPPO	1324	6	S4/R2	E4-E6-E9	456
2	S1/R4	E3-E4-E6	1258	7	S3/R1	E5-E12 (E9X)	736
3	S2/R3	E3-E4-E5	445	8	S3/R2	E5-E9	515
4	S2/R2	E3-E9 (E5X)	818	9	S5/R1	E9-E12	339
5	S2/R1	E3-E12 (E5X,E9X)	1039	10	S2/R4	E3-E4-E6	379

Fig.4


A
C
tc
B
fp
hb
hc
mb
dc
tc
C
sc
nc
D
tc
mb
hb
ot
dc
r2 r3 r4 r5
E
sc
fp
nc
F
G
r2
H

Fig.5

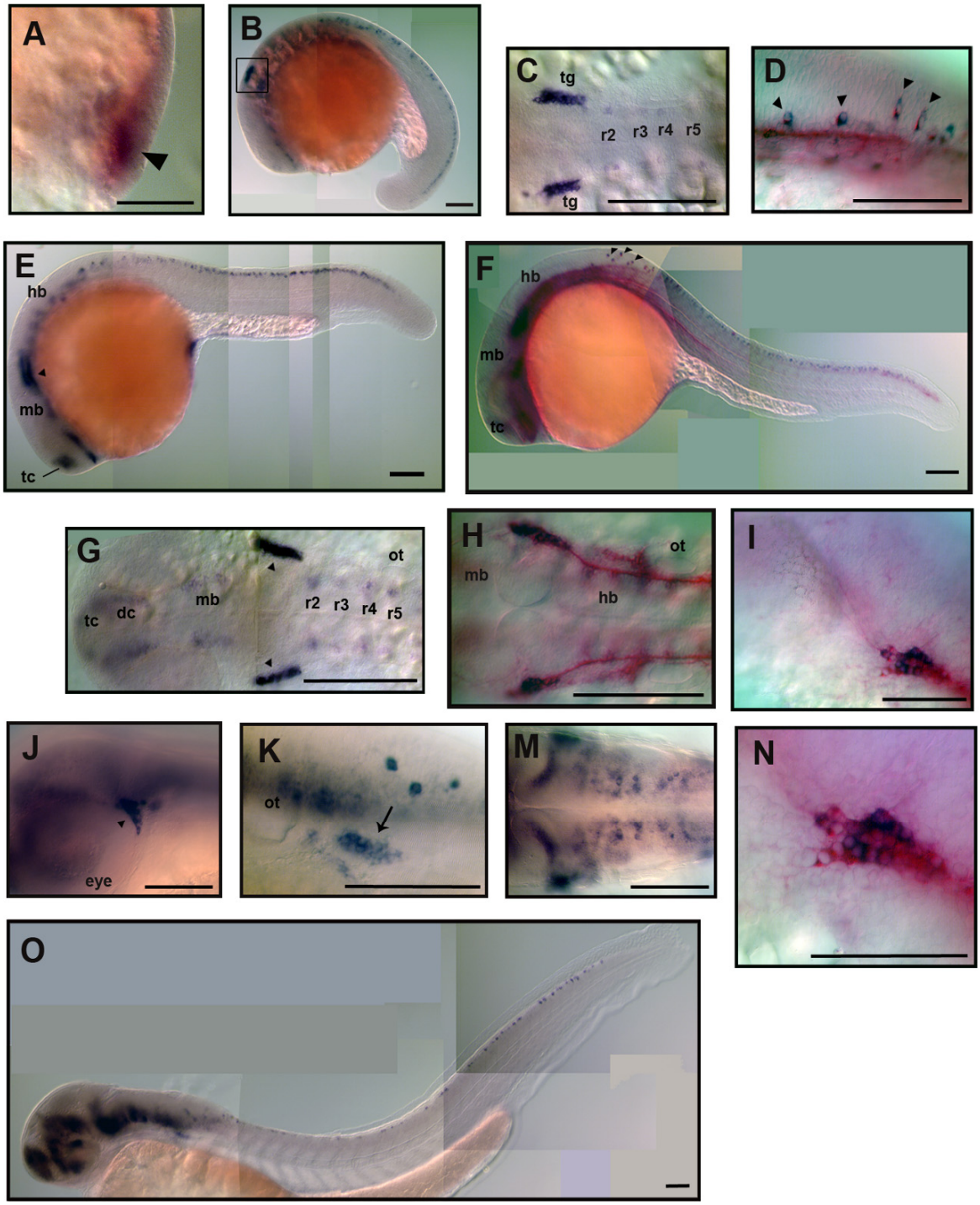
A
B
C
tg
r2 r3 r4 r5
tg
D
E
hb
mb
tc
F
hb
mb
tc
G
ot
tc dc
mb
r2 r3 r4 r5
H
ot
mb
hb
I
J
eye
K
ot
M
N
O

Fig.6

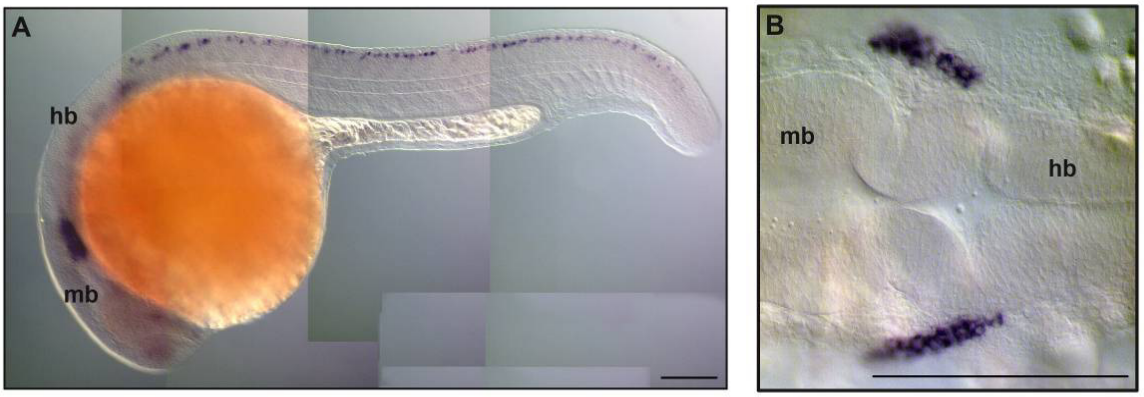

Chapter III

Research Paper II

Analysis of the function of endogenous Tau proteins in zebrafish (A thesis chapter in the form of an incomplete manuscript)

Authors:

Mengqi Chen[1,*], Ralph N. Martins[2,3,4] and Michael Lardelli[1],

Affiliations:

1. Zebrafish Genetics Laboratory, Discipline of Genetics, School of Molecular and Biomedical Sciences, The University of Adelaide, Adelaide SA 5005, Australia.

2. Centre of Excellence for Alzheimer's Disease Research and Care, School of Exercise, Biomedical and Health Sciences, Edith Cowan University, Joondalup, WA 6027, Australia.

3. Sir James McCusker Alzheimer's Disease Research Unit, Hollywood Private Hospital, Nedlands, WA 6009, Australia.

4. School of Psychiatry and Clinical Neurosciences, University of Western Australia, Crawley, WA 6009, Australia.

*** Corresponding author:**

Mengqi Chen, Zebrafish Genetics Laboratory, School of Molecular and Biomedical Sciences, The University of Adelaide, Adelaide SA 5005, Australia. Tel. (+61 8) 83034863, Fax. (+61 8) 83034362, email: mengqi.chen@adelaide.edu.au

STATEMENT OF AUTHORSHIP

Analysis of the function of endogenous Tau proteins in zebrafish

(unsubmitted manuscript)

Mengqi Chen (Candidate)

Performed all experimentation. Wrote the manuscript.

Signed

Ralph N. Martins (co-author)

Provided funding for the project.

Signed

Michael Lardelli (co-author)

Planned the research and supervised the development of the work. Edited the paper.

Signed

Abstract

Tau protein has been implicated in numerous neurodegenerative diseases, including Alzheimer's disease (AD) and frontotemporal dementia with parkinsonism linked to chromosome 17 (FTDP-17). There are two tau paralogues, *mapta* and *maptb*, in zebrafish. We have developed polyclonal antibodies that allowed specific detection of each tau protein. In addition, we have investigated their function during embryogenesis using translation inhibiting morpholino oligonucleotides. Inhibition of the Mapta translation causes distortion of the rostrocaudal axis, whereas, inhibition of Maptb leads to impaired axonogenesis from trigeminal ganglion and/or reduced size of this structure. To complete this manuscript, rescue experiments would be required to confirm whether the phenotypes observed are specifically caused by lack of tau function and to indicate the amount of functional redundancy that exists between Mapta and Maptb.

Key words: Tau, Zebrafish, Phenotype

Introduction

Tau is a microtubule associated protein that predominantly expresses in the nervous system. The major function of the tau protein is to stabilize and regulate the dynamics of microtubules [1]. In adult human brain, the single *tau* gene produces two classes of tau isoforms with either 3 or 4 tubulin-binding repeats in their C-termini (referred as 3R-tau and 4R-tau) through alterative splicing of exon 10 [2]. The inclusion of the additional tubulin-binding motif in 4R-tau increases its ability to associate with microtubules by ~2-fold compared to 3R-tau [3, 4]. Normally, a 1:1 ratio between these two classes of tau isoforms is precisely maintained in adult human brain [5]. In addition to the alterative splicing of exon 10, the affinity

between tau proteins and microtubules is also modulated by phosphorylation, which detaches tau from microtubules [5].

Tau function appears to be essential for maintenance of neuron morphology, axonal plasticity, and intracellular transportation [6]. Dysfunction of tau has been observed in numerous neurodegenerative diseases known as tauopathies, including Alzheimer's disease (AD) and frontotemporal dementia with parkinsonism linked to chromosome 17 (FTDP-17) [1]. In these diseases, abnormal hyperphosphorylated tau filaments accumulate in the cell body of neurons to form insoluble deposits. The aberrant hyperphosphorylation of tau is correlated with dysregulation of tau-related kinases and phosphatases [7]. Additionally, isoform profiles of tau proteins are disturbed in a disease-specific manner in most tauopathies [2]. Direct evidence for the causative relationship between tau dysfunction and tauopathy came from the identification of several mutations in the *tau* gene in cases of FTD showing autosomal dominant inheritance [8, 9]. However, the detailed mechanism of how the dysfunction of tau leads to neurodegeneration remains unclear.

Zebrafish embryos have been demonstrated to be a powerful animal model for investigation of the genetics and pathological mechanisms of human diseases. Previously, we identified two tau paralogues, *mapta* and *maptb*, in zebrafish. As for the human *MAPT* gene, transcripts of these genes undergo complex alterative splicing. Interestingly, the *mapta* gene encodes tau proteins with 4 to 6 tubulin binding motifs (4-6R) while the *maptb* gene predominantly produces tau proteins with 3 tubulin binding motifs (3R). In this study, we examined the function of both genes during embryogenesis. Mopholino antisense oligonucleotides (MOs) were used to inhibit the translation of both genes and polyclonal antibodies for detection of Mapta and Maptb specifically were developed. Inhibition of Mapta translation resulted in distortion of the rostrocaudal axis, whereas, inhibition of Mapt

translation impaired axonal outgrowth from the trigeminal ganglion similar to that observed in tau knock-out mice [10]. Trigeminal ganglion size was also reduced suggesting reduced neuron number. These findings support the use of the zebrafish as a model for the analysis of tau function, especially in axonogenesis.

Results

Validation of MOs for inhibition of *mapta* mRNA translation *in vivo*

To determine the function of *mapta* and *maptb* in zebrafish development, we designed two distinct morpholino oligonucleotides (MOs) targeting the 5' UTR and start codon region for *mapta* and three MOs targeting *maptb*.

We validated the function of the *mapta* MOs by the following strategy: The MO binding regions of *mapta* were cloned and fused in frame to the Green Fluorescent Protein gene (GFP) downstream at a cytomegalo-virus (CMV) promoter in the PEGFP-N1 vector. Injection of this vector at a concentration of 67ng/µl results in expression of GFP. Co-injection of this vector with negative control MO did not affect GFP expression. However, co-injection with any of the MOs inhibiting translation inhibited the expression of GFP (data not shown). This supports that the MOs can bind to *mapta* mRNA to inhibit its translation.

A similar strategy could not be used to test the function of MOs designed to inhibit translation of *maptb* since fusion of *maptb* 5' sequences to GFP appeared to inhibit GFP expression. This was confirmed by subsequent deletion of these sequences from the vector that reinstated GFP expression.

Detection of Mapta and Maptb protein by western blotting

To detect specifically Mapta or Maptb proteins, two polyclonal antibodies were raised from goats. The antigens used for both antibodies were synthetic 15 amino acid peptide sequences derived from areas of sequence unique to each protein (see Materials and Methods).

Mapta and Maptb proteins in embryos at 24hpf were analyzed by western blotting. As shown in Fig1.A, the antibody against Mapta (Abmapta) detected two bands at ~48kDa and ~52kDa. Injection of *in vitro* synthesized mRNA encoding a 369 amino acid isoform of Mapta increased the ~48kDa band. In contrast, injection of the translation inhibiting MOs, TMOmapta1 and TMOmapta2, greatly reduced the signal of the ~48KD band. In addition, injection of TMOmapta2 also reduced the signal of the ~52KD band obviously, whereas, the reduction of signal strength of the ~52KD band by injection of TMOmapta1 was minor. The predicted molecular weights of Mapta protein isoforms range from 35 to 42kDa. Therefore, Mapta shows retarded mobility in SDS PAGE possibly due to post-translational modification.

The Maptb antibody also detected two bands at ~50kDa and ~60kDa. The ~50kDa band is stronger than the ~ 60kDa band. Injection of the translation inhibiting MO, TMOmaptb1, at a concentration of 0.5mM suppressed the ~ 50kDa band completely and reduced the level of the ~ 60kDa band significantly, while injection of the second MO, TMOmaptb2, only partially blocked Maptb translation. The third MO, TMOmaptb3, failed to affect the level of either band (Fig1.B). Like Mapta, Maptb proteins also lagged ~ 15kDa behind the position of their predicted molecular weight in SDS PAGE.

A distorted rostrocaudal axis caused by injection of *mapta* MOs at high concentration

To assess the role of Mapta during embryonic development, embryos were injected with translation inhibiting MOs, TMOmapta1 or TMOmapta2, at the one cell stage and then stained by in situ transcript hybridization with a *mapta* cRNA probe to show the hypochord and floorplate. Injection of either MOs at a high concentration (1mM) caused distortion of the rostrocaudal axis including the notochord (Fig2). In embryos injected with TMOmapta1, the notochord showed a distinct kinking phenotype in the trunk region (Fig2. D, F). In addition, the somites lost their typical chevron V-shape (Fig2.B), but exhibited a U-shaped form (Fig2.E). Injection of a second translation inhibiting MO, TMOmapta2, also induced the abnormal notochord distortion phenotype, but less severely than that caused by TMOmapta1. In addition, the distortion occurred in a relatively more caudal region compared to that induced by TMOmapta1 (Fig2.G, I). The somites were also misshapen, forming gaps at somite boundaries (Fig2.H). These phenotypes could not be observed when the injection concentration of translation inhibiting MOs was reduced to 0.5mM or lower (data not shown). In addition, co-injection of synthesized mRNA that encoded a 5R Mapta isoform failed to rescue the phenotype. Therefore, it remains unclear whether this phenotype is caused by specifically reduced mapta function.

Inhibition of *maptb* translation results in impairment of axonal outgrowth and trigeminal ganglion size

To determine the morphological changes induced by loss of maptb function, embryos were injected with translation inhibiting MOs TMOmaptb1 or TMOmaptb2 at the one cell stage. Injection of the standard negative control morpholino (a 25bp oligonucleotide that is unable to bind the 5'UTR region of the target mRNAs) at the same concentration did not induce any visible phenotype. However, injection of TMOmaptb1 (Fig3.A, B) but not

TMOmaptb2 (data not shown) led to expansion of the ventricular space in the region at the midbrain in a dose-dependent manner at 48hpf as follow: 0.5mM, 96.4±1.7% (SEM, n=110) ; 0.25mM, 55.7±4.6% (SEM, n=83).

Since our previous study indicated strong expression of *maptb* transcripts in the trigeminal ganglion, we examined whether inhibition of Maptb translation would induce any phenotypic effects in this region. We injected embryos with either TMOmaptb1 or TMOmaptb2 and then fixed them at 24hpf. We then stained these embryos with the antibody zn12 that labels a set of specific neurons including those of the trigeminal ganglion [11]. The injection of the control or translation inhibiting MOs and the subsequent fixation and staining was performed so as to maximize the comparability of the staining intensity (see [22]). For example, control and experimental embryos were stained in the same tubes. Injection of either translation inhibiting MO resulted in remarkable impairment of axonal outgrowth, judging by the apparent axonal length and branch density (Fig3. C-E). In addition, the number of trigeminal ganglion neurons appeared to be reduced in TMOmaptb1-injected embryos (Fig3.D) judging by the overall size of the trigeminal ganglion. The trigeminal ganglion size phenotype induced by injection of TMOmaptb2 was relatively less severe than that caused by TMOmaptb1 and a similar but less severe impairment of axonal development was also observed (Fig3.E).

The observation that the two distinct MOs produce a similar phenotype of impaired axonal development from the trigeminal ganglion supports that the conclusion that the phenotype is specifically due to loss of Maptb function. However, we were unable to rescue the phenotype by injection of *maptb* mRNA. In fact, we were also unable to observe any elevation in Maptb protein after injection of the synthesized *maptb* mRNA (data not shown), indicating a failure to force expression of this protein.

Discussion and further work to complete the manuscript

This study indicated a possible important role for Maptb in the axonal development of trigeminal ganglion neurons during zebrafish embryogenesis. Maptb also appeared to influence the size of the trigeminal ganglion. Our previous study identified two tau paralogues, *mapta* and *maptb*, in zebrafish. The *mapta* gene encodes isoforms of tau with 4 to 6 tubulin-binding domains (4R-6R), whereas, the *maptb* gene is predominantly translated into 3R-tau isoforms. Given the strong correlation of disrupted 4R/3R balance with various neurodegenerative disorders [2], the zebrafish appears to be a valuable model for investigating the functions of these two varieties of tau isoform. This may provide insights into how changes in the ratio between 4R and 3R-tau isoforms contribute to neurodegeneration.

Zebrafish embryos are highly tractable for genetic manipulation. The expression levels of particular genes can be readily reduced by injection of MOs, or increased by injection of synthetic mRNA during embryogenesis. We designed and injected two translation inhibiting MOs targeting different region of the *mapta* gene and three blocking *maptb*. The ability of the MOs to inhibit *mapta* expression was supported by their ability to inhibit expression of GFP by interacting with MO binding sites that had been fused upstream of the GFP start codon. Unfortunately, we were unable to test the MOs for *maptb* in the same way, because fusion of the MO binding site of *maptb* to GFP coding sequences in the pEGPF-N1 vector alone inhibited the expression of GFP.

Two polyclonal antibodies were developed for specific detection of Mapta (Abmapta) and Maptb (Abmaptb). The Abmapta antibody detected two bands.

These exhibited a ~10kDa larger molecular weight than predicted theoretical translation of coding sequence. Injection of translation inhibiting MOs at a concentration of 1mM reduced the level of both bands, while injection of mRNA encoding a 5R Mapta isoform increased the concentration of the ~48kDa band, indicating that both bands represent tau isoforms. The Abmaptb antibody also detected two bands. Similarly, these two bands were retarded by ~15kDa compared to their expected migration in SDS PAGE on 11% gels. The level of the ~50kDa isoform of Maptb was markedly higher than the ~60kDa isoform in 24hpf wildtype embryos. In addition, the ~50kDa isoform appeared to be more sensitive to inhibition by TMOmaptb1 compared to the ~60kDa isoform. The retarded migration of tau proteins in SDS PAGE has been reported for tau from humans, mice, and frogs [12-15], although the size shift of tau in those organisms is less extreme relative to zebrafish Mapta/b. The retarded migration may be due to secondary structure and posttranslational modification of the Mapt proteins.

Evidence for a role of tau protein in axongenesis has been found in several studies both *in vitro* and *in vivo* [10, 16, 17], although there are some contradictory results supporting that tau function is redundant for neuron maturation [18, 19]. In this study in zebrafish, we have shown that inhibition of Maptb translation impairs axonal outgrowth from the trigeminal ganglion neurons and/or reduces the number of neurons in this structure (i.e. we cannot be sure whether or not this is just due to having less neurons). Our previous study showed that only *maptb*, which encodes predominantly the 3R-tau protein isoforms, is expressed in this region. This implies that 3R-tau but not 4-6R-tau may be essential for axonal outgrowth and/or neuronal formation/survival.

The phenotype induced by TMOmaptb1 appears to be more severe than that produced by TMOmaptb2. This is consistent with the observation that

TMOmaptb1 is more effective in inhibiting the expression of Maptb (Fig1.B). The higher efficiency of TMOmaptb1 may also explain the observation that only TMOmaptb1 caused a ventricular expansion phenotype. However, we have not yet successfully rescued any phenotype caused by MOs targeting maptb, because the synthetic mRNAs encoding *maptb* or coding sequences containing *maptb* 5' sequences fail to express in zebrafish embryos. We currently cannot explain this phenomenon.

Injection of MOs inhibiting of the translation of *mapta* induces a disrupted rostrocaudal axis phenotype with a distorted notochord and disorganized somites. However, this is only seen at the highest injection concentration. Although we failed to rescue the phenotype by injection of synthetic mRNA encoding a 5R isoform of Mapta, the phenotype was observed in embryos injected with two different MOs. However, since the MOs share 11 bases of overlapping sequence, we cannot be certain that the common phenotype they cause is specific to their action on *mapta*. This phenotype, if specifically due to loss of Mapta activity, may be related to the observed expression of *mapta* mRNA protein in the hypochord and floorplate.

Further study would focus initially on the rescue of phenotypes produced by *maptb* MOs via an alterative strategy. A cDNA encoding the large isoform of *maptb* (but engineered not to bind the translation-inhibiting MOs) would be inserted into the efficient tol-2 transposon vector. Injection of this construct may induce mosaic expression of exogenous Maptb protein to the extent that it could partially rescue the phenotype of impaired axongenesis and/or ganglion size caused by *maptb* MOs in the trigeminal ganglion. Furthermore, we would also try to rescue this phenotype by *mapta* expression via the same method. The results of this strategy might not only confirm the specificity of the MO phenotype, but also indicate the amount of redundancy that exists in Mapta and Maptb function.

Material and Methods

Generation of vectors

To validate the function of MOs for *mapta*, we constructed a plasmid, pEGFP-N1-maptaMO, in which the binding sequence of mapta MOs is fused in frame upstream of EGFP. The MO binding sequence was amplified from cDNA from 24hpf embryos by RT-PCR using primer pairs 5'-cggaattcGGAGAGACAATAACAGCGACG-3' and 5'-ggggtaccTAGTGAGCATTGGGCGAGGAG-3' (Upper case letters indicate *mapta* sequence. Lower case sequence contains additional restriction sites.). The cDNA fragment was then inserted into the pEGFP-N1 vector (BD Biosciences, NJ, USA) using restriction sites EcoRI and KpnI.

To construct the template plasmids, pcGlobin2-mapta1 and pcGlobin2-maptb2, for synthesis of *mapta* and *maptb* mRNA respectively, cDNA fragments encoding a 369 amino acid isoform of mapta and a 367 amino acid isoform of the maptb protein were amplified from full-length open reading frames of isoforms of these genes in the pGEM-T vector (Promega Crop., Madison, WI, USA). Primer pairs used were: 5’-ggaattcaccATGGACCAGCACCACGATTT-3’ and 5’-ccgctcgagTCA CAAGCCCTGTTTGGCG-3’ for *mapta* and 5’-tccccgcggaccATGGACCATCAGGACCAC-3’ and 5’-ccgctcgagCTT TTCTGGATTCGTCAG-3’ for *maptb*. The fragments were cleaved with EcoRI and XhoI or SacII and XhoI respectively before ligation into the pcGlobin2 vector [20].

Production of antibodies

Polyclonal antibodies were ordered from Genscript (GenScript Corporation, NJ, USA). The antigen used for zebrafish Mapta was a synthetic C-terminal amidated peptide corresponding to the C-terminal epitope CDHGAEIVSLEESPQ, while the antigen used for Maptb was a N-terminal acetylated peptide corresponding to the epitope PGSIERADSPKTPDC in the proline rich region of that protein. The antigens were used to immunize goats and resultant sera were affinity purified.

Westernblotting

Protein samples were prepared as previously described [21]. The Mapta isoforms were separated on 12% SDS-polycrylamide gels, while the Maptb isoforms were separated on 11% SDS gels. Proteins were transferred to nitrocellulose membranes. The membranes were blocked with 10% w/v skim milk powder in TBST at 4℃ overnight before incubating with a 1/1000 dilution of primary antibody in TBST containing 1% w/v skim milk for 2 hours at room temperature. The membranes were then washed in TBST and incubated with a 1/7500 dilution of donkey antigoat IgG (Jackson ImmunoResearch Laboratories, Inc., Baltimore, PA, USA) for 1 hour. Detection of β-tubulin as a loading control was performed as previously descirbed [21]. After incubation with secondary antibodies, all membranes were washed four times in TBST and visualized using X-ray film with chemiluminescence as previously described [21].

RNAs and MOs injections

Morpholino oligonucleotides (MOs) were purchased from Gene Tools (LLC, Corvallis, OR, USA). Two anti-*mapta* MOs and three anti-*maptb* MOs were designed against the start regions of the mRNAs as follow:

TMOmapta1, AGCAAGTCCAAACGAGGATACTGTG;

TMOmapta2, TGGTGCTGGTCCATAGCAAGTCCAA;

TMOmaptb1, CATGTGGTCCTGATGGTCCATTTTG;

TMOmaptb2, TGAGATGATTTCAGTCTCTGTAGCA;

TMOmaptb3, AGATGATTTCAGTCTCTGTAGCACA;

The standard negative control Mo sequence was as follows: CCTCTTACCTCAGTTACAATTTATA. MOs solutions and dilutions for injection were prepared as previously described and were injected into embryos at the 1 or 2 cell stage [22].

Capped mRNAs were synthesized from expression vectors pcGlobin2-mapta1 and pcGlobin2-maptb2, using the T7 mMessage mMachine kit (Ambion Inc., Austin, TX, USA). Approximately 2nl of RNA at experimental MO concentrations ranging from 0.25mM to 1mM was injected into embryos at the 1 or 2 cell stage. However, all MO injections were performed at a total concentration of 1mM by adding negative control MO to experimental MO where necessary [22]

Whole-mount immunohistochemistry

For whole-mount immunohistochemistry, zebrafish embryos were fixed in 4% formaldehyde in TBST overnight at 4℃. The fixed embryos were washed 3X5 min in TBST and incubated in ice cold acetone for 7 mins. After permeabilization in acetone, embryos were washed 4X5 min in TBST and incubated for 1hr in block reagent (Roche Diagnostics GmbH, Mannheim, Germany) at room temperature before incubating in zn12 antibody [11] at a dilution of 1:200 overnight at 4℃. The embryos were washed 4X15 min at room temperature and incubated in AP-anti-mouse antibody (Rockland Immunochemicals, Inc., Gilbersville, PA, USA) for 4hrs at room temperature. After that, the embryos were washed 4X15 min at room temperature and then

stained using BCIP/NBT as previously described [23].

Whole-mount in situ hybridization

Whole-mount in situ hybridization was conducted according to [24], using single-stranded antisense RNA probes labelled with digoxigenin-UTP. The probes were synthesized using T7 RNA polymerase from PCR fragments amplified using M13 primers and the p-GEM-T-mapta1 plasmid as a template.

Acknowledgement:

This work was supported by a Project Grant (453622) to M. Lardelli and R.N. Martins from the National Health and Medical Research Council of Australia. Animal experimentation was carried out under the auspices of the Animal Ethics Committee of the University of Adelaide.

Fig1

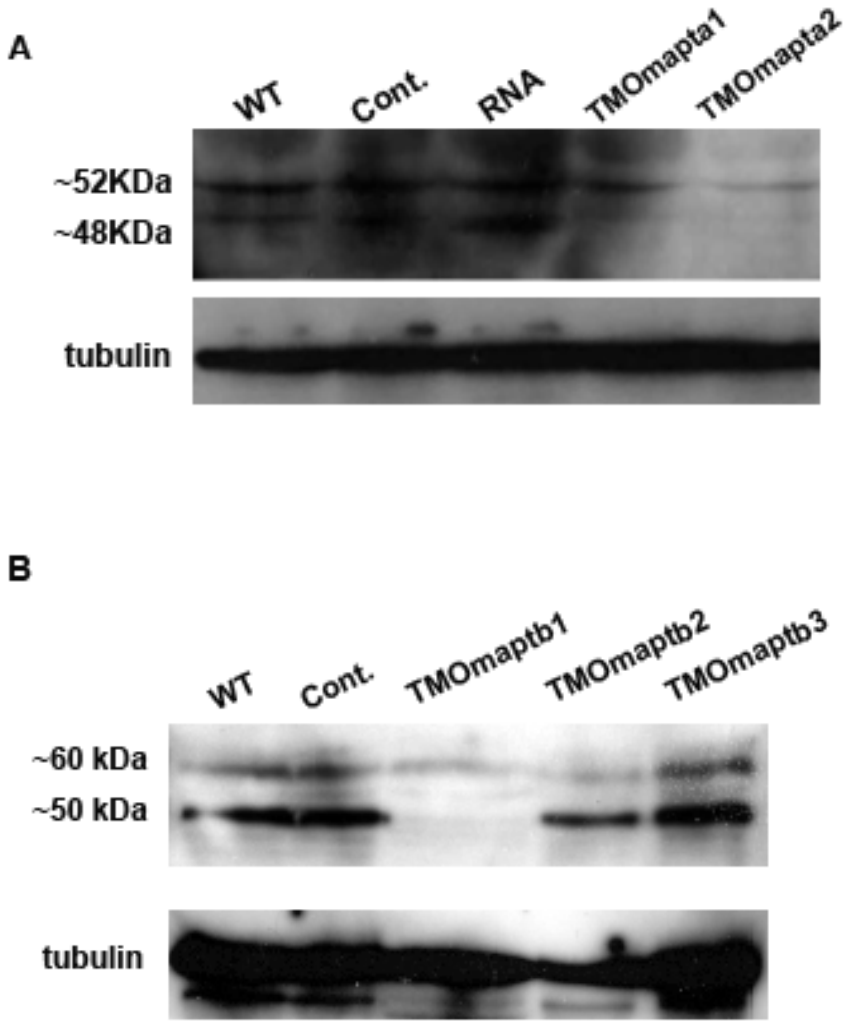
A
WT
Cont.
RNA
TMOmapta1
TMOmapta2
~52KDa
~48KDa
tubulin
B
WT
Cont.
TMOmaptb1
TMOmaptb2
TMOmaptb3
~60 kDa
~50 kDa
tubulin

Fig2

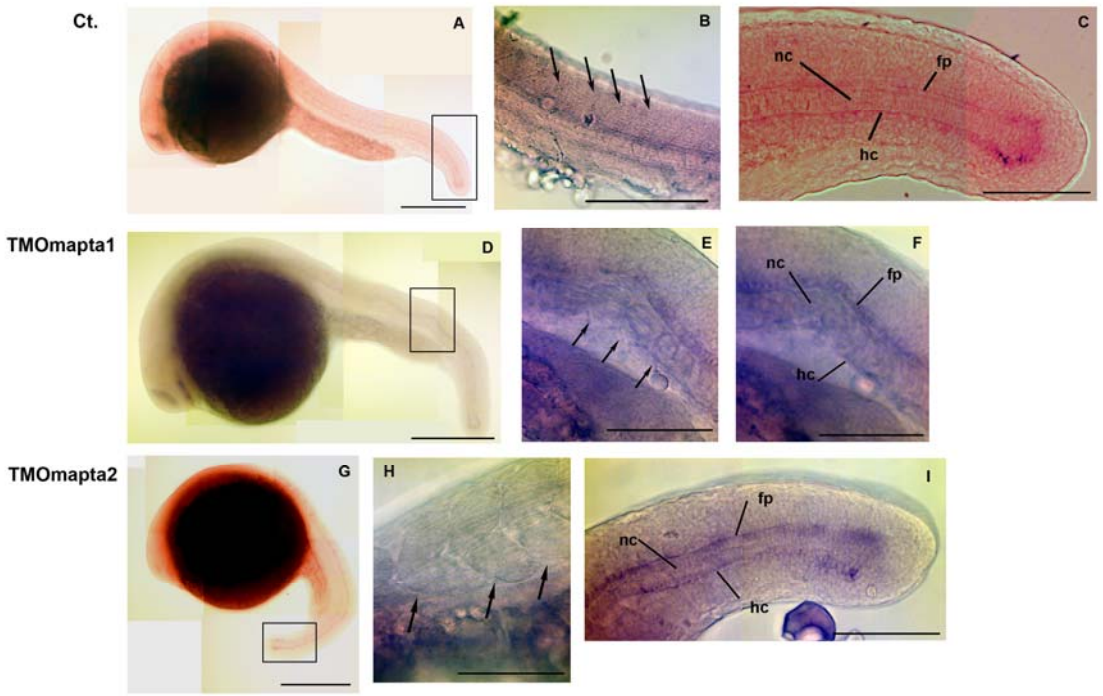

Fig3

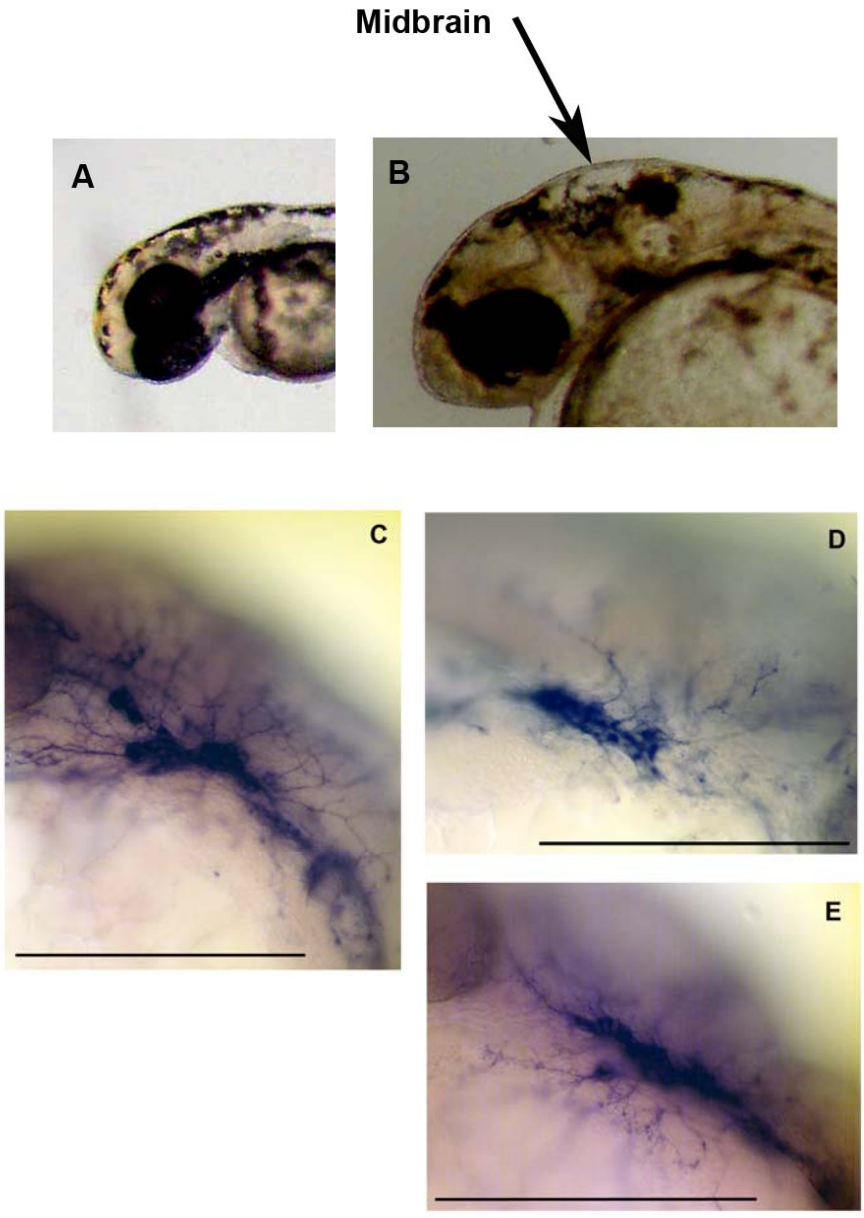

Fig Legend

Fig1. Tau expression in zebrafish embryos at 24hpf. **(A)** The Abmapta antibody detected bands at ~52kDa and ~48kDa on an immunoblot (Lane 1). Injection of standard negative control MO did not affect Mapta expression (Lane 2). Injection of a synthetic mRNA encoding a 369 amino acid isoform of Mapta increased the density of the ~48kDa band (Lane 3). Injection of either translation inhibiting MOs at a concentration of 1mM partially inhibited expression of both bands (Lane 4, 5). **(B)** The Abmaptb antibody detected bands at ~50kDa and ~60kDa from wildtype embryos. (Lane 1). Injection of a control MO did not affect the level of Maptb (Lane 2). Injection of translation inhibiting MO TMOmaptb1 at a concentration of 0.5mM suppressed the ~50kDa band completely and reduced the ~60kDa band significantly (Lane 2). Injection of TMOmaptb2 partially reduced both bands (Lane 4)., whereas, injection of TMOmaptb3 did not affect the expression level of Maptb (Lane 5).

Fig2. Distorted notochord and disorganized somites associated with injection of MOs blocking translation of Mapta at a concentration of 1mM. Embryos were stained using *mapta* cRNA probes at 24hpf. Anterior to the left. **(A-C)** Embryos injected with negative control MO show a straight notochord and V-shaped somites. Black box indicates area showing in **(C)**. Black arrows indicate the V-shaped normal somites. (**D-F**) Embryo injected with TMOmapta1. **(D)** Lateral view showing kinked distortion of notochord in trunk region. Black box shows area represented in **(F)**. **(E)** Lateral view. Black arrows indicate the abnormal U-shaped somites. **(F)** Lateral view showing the distorted notochord and the floorplate. **(G-I)** Embryos injected with TMOmapta2. **(G)** Lateral view showing distorted notochord in the tail region. The black box shows the area represented in **(I)**. **(H)** Lateral view with black arrows showing misshaped somites and gaps in the somite boundary region. **(I)** Lateral view exhibiting distorted notochord. Size bars indicate 50μm. *Abbrevations:* fp, floor plate; hc, hypochord; nc, Notochord.

Fig3. Phenotypic change associated with injection of MO blocking translation of Maptb. **(A-B)** Ventricular expansion in the midbrain region resulting from injection of TMOmaptb1 **(B, black arrow)** compared with control-injected embryos at 48hpf **(A)**. **(C-E)** Impaired axonal outgrowth of trigeminal ganglion neurons due to injection of TMOmaptb1/2 compared to control-injected embryos. The trigeminal ganglia were stained using zn12 antibody at 24hpf. **(C)** Lateral view of negative control-injected embryos. **(D)** Lateral view of TMOmaptb1-injected embryos showing apparantly decreased branch density and axonal length of trigeminal ganglion neurons and reduced number of trigeminal ganglion neurons compared to control. **(E)** Lateral view of TMOmaptb2-injected embryo showing impaired axongenesis. Size bars

indicate 100μm.

References:

[1] R. Brandt, M. Hundelt, N. Shahani, Tau alteration and neuronal degeneration in tauopathies: mechanisms and models, Biochimica et biophysica acta 1739 (2005) 331-354.

[2] A. Andreadis, Tau gene alternative splicing: expression patterns, regulation and modulation of function in normal brain and neurodegenerative diseases, Biochimica et biophysica acta 1739 (2005) 91-103.

[3] K.A. Butner, M.W. Kirschner, Tau protein binds to microtubules through a flexible array of distributed weak sites, The Journal of cell biology 115 (1991) 717-730.

[4] B.L. Goode, M. Chau, P.E. Denis, S.C. Feinstein, Structural and functional differences between 3-repeat and 4-repeat tau isoforms. Implications for normal tau function and the onset of neurodegenetative disease, The Journal of biological chemistry 275 (2000) 38182-38189.

[5] C. Ballatore, V.M. Lee, J.Q. Trojanowski, Tau-mediated neurodegeneration in Alzheimer's disease and related disorders, Nature reviews 8 (2007) 663-672.

[6] J.Z. Wang, F. Liu, Microtubule-associated protein tau in development, degeneration and protection of neurons, Progress in neurobiology 85 (2008) 148-175.

[7] W.H. Stoothoff, G.V. Johnson, Tau phosphorylation: physiological and pathological consequences, Biochimica et biophysica acta 1739 (2005) 280-297.

[8] M. Hutton, C.L. Lendon, P. Rizzu, M. Baker, S. Froelich, H. Houlden, S. Pickering-Brown, S. Chakraverty, A. Isaacs, A. Grover, J. Hackett, J. Adamson, S. Lincoln, D. Dickson, P. Davies, R.C. Petersen, M. Stevens, E. de Graaff, E. Wauters, J. van Baren, M. Hillebrand, M. Joosse, J.M. Kwon, P. Nowotny, L.K. Che, J. Norton, J.C. Morris, L.A. Reed, J. Trojanowski, H. Basun, L. Lannfelt, M. Neystat, S. Fahn, F. Dark, T. Tannenberg, P.R. Dodd, N. Hayward, J.B. Kwok, P.R. Schofield, A. Andreadis, J. Snowden, D. Craufurd, D. Neary, F. Owen, B.A. Oostra, J. Hardy, A. Goate, J. van Swieten, D. Mann, T. Lynch, P. Heutink, Association of missense and 5'-splice-site mutations in tau with the inherited dementia FTDP-17, Nature 393 (1998) 702-705.

[9] L.N. Clark, P. Poorkaj, Z. Wszolek, D.H. Geschwind, Z.S. Nasreddine, B. Miller, D. Li, H. Payami, F. Awert, K. Markopoulou, A. Andreadis, I. D'Souza, V.M. Lee, L. Reed, J.Q. Trojanowski, V. Zhukareva, T. Bird, G. Schellenberg, K.C. Wilhelmsen, Pathogenic implications of mutations in the tau gene in pallido-ponto-nigral degeneration and related neurodegenerative disorders linked to chromosome 17, Proceedings of the National Academy of Sciences of the United States of America 95 (1998) 13103-13107.

[10] H.N. Dawson, A. Ferreira, M.V. Eyster, N. Ghoshal, L.I. Binder, M.P. Vitek, Inhibition of neuronal maturation in primary hippocampal neurons from tau deficient mice, Journal of cell science 114 (2001) 1179-1187.

[11] B. Trevarrow, D.L. Marks, C.B. Kimmel, Organization of hindbrain segments in the zebrafish embryo, Neuron 4 (1990) 669-679.

[12] M. Goedert, M.G. Spillantini, R. Jakes, D. Rutherford, R.A. Crowther, Multiple isoforms of human microtubule-associated protein tau: sequences and localization in neurofibrillary tangles of Alzheimer's disease, Neuron 3 (1989) 519-526.

[13] L.I. Binder, A. Frankfurter, L.I. Rebhun, The distribution of tau in the mammalian central nervous system, The Journal of cell biology 101 (1985) 1371-1378.

[14] J.C. Larcher, D. Boucher, I. Ginzburg, F. Gros, P. Denoulet, Heterogeneity of Tau proteins during mouse brain development and differentiation of cultured neurons, Developmental biology 154 (1992) 195-204.

[15] O.F. Olesen, H. Kawabata-Fukui, K. Yoshizato, N. Noro, Molecular cloning of XTP, a tau-like microtubule-associated protein from Xenopus laevis tadpoles, Gene 283 (2002) 299-309.

[16] A. Caceres, K.S. Kosik, Inhibition of neurite polarity by tau antisense oligonucleotides in primary cerebellar neurons, Nature 343 (1990) 461-463.

[17] C.W. Liu, G. Lee, D.G. Jay, Tau is required for neurite outgrowth and growth cone motility of chick sensory neurons, Cell motility and the cytoskeleton 43 (1999) 232-242.

[18] A. Harada, K. Oguchi, S. Okabe, J. Kuno, S. Terada, T. Ohshima, R. Sato-Yoshitake, Y. Takei, T. Noda, N. Hirokawa, Altered microtubule organization in small-calibre axons of mice lacking tau protein, Nature 369 (1994) 488-491.

[19] I. Tint, T. Slaughter, I. Fischer, M.M. Black, Acute inactivation of tau has no effect on dynamics of microtubules in growing axons of cultured sympathetic neurons, J Neurosci 18 (1998) 8660-8673.

[20] H. Ro, K. Soun, E.J. Kim, M. Rhee, Novel vector systems optimized for injecting in vitro-synthesized mRNA into zebrafish embryos, Molecules and cells 17 (2004) 373-376.

[21] S. Nornes, C. Groth, E. Camp, P. Ey, M. Lardelli, Developmental control of Presenilin1 expression, endoproteolysis, and interaction in zebrafish embryos, Experimental cell research 289 (2003) 124-132.

[22] S. Nornes, M. Newman, G. Verdile, S. Wells, C.L. Stoick-Cooper, B. Tucker, I. Frederich-Sleptsova, R. Martins, M. Lardelli, Interference with splicing of Presenilin transcripts has potent dominant negative effects on Presenilin activity, Human molecular genetics 17 (2008) 402-412.

[23] R. Tamme, S. Wells, J.G. Conran, M. Lardelli, The identity and distribution of neural cells expressing the mesodermal determinant spadetail, BMC developmental biology 2 (2002) 9.

[24] R. Tamme, K. Mills, B. Rainbird, S. Nornes, M. Lardelli, Simple, directional cDNA cloning for in situ transcript hybridization screens, BioTechniques 31 (2001) 938-942, 944, 946.

Significance of the Research Project and Future Directions

As a consequence of longer life expectancy and an aging population, the impact of tauopathies is expected to grow, placing a heavy burden on health care resources. Effective therapies and diagnostic methods are not yet available for this disease. To help the development of such therapies, research on the mechanism(s) underlying tauopathies is needed.

The zebrafish embryo has been demonstrated to be a valuable animal model for analyzing the mechanism of tauopathies. This study on the endogenous tau gene of zebrafish provided important information on the cell biology and function of native zebrafish tau. The development of antibodies to zebrafish tau allowed the specific detection of the two tau proteins, which will underpin further mechanistic studies of tauopathies in zebrafish. Moreover, the discovery of the separation of expression of 3R and 4-6R tau between two *mapt* genes in zebrafish suggests that the zebrafish embryo may be a powerful animal model in which investigate the still enigmatic pathological role of altered tau isoform profile in the development of tauopathies.

Future directions for further investigation of Mapt function were discussed in Paper II. The altered isoform ratio of tau is a character of multiple tauopathies. However, how this change of isoform profiles affect tau function is poorly understood. Zebrafish expresses 3R and 4-6R tau isoforms in different genes. Therefore, it might be interesting to investigate whether the alteration of the ratio between Mapta and Maptb leads to neurodegeneration. This might be accomplished using transgenic zebrafish that express siRNAs against *mapta* or *maptb* mRNA conditionally. In addition, the method we have established to analyse zebrafish endogenous tau in axonogenesis may be applied to any further studies of the molecular mechanisms underlying tauopathies in the zebrafish model.